

This is an Open Access document downloaded from ORCA, Cardiff University's institutional repository: <https://orca.cardiff.ac.uk/id/eprint/160601/>

This is the author's version of a work that was submitted to / accepted for publication.

Citation for final published version:

Tang, Chao, Wang, Peng, Zhu, Xiaoxuan, Qi, Kaijie, Xie, Zhihua, Zhang, Hao, Li, Xiaoqiang, Gao, Hongru, Gu, Tingting, Gu, Chao, Li, Shan, de Graaf, Barend H. J. , Zhang, Shaoling and Wu, Juyou 2023. Acetylation of inorganic pyrophosphatase by S-RNase signaling induces pollen tube tip swelling by repressing pectin methylesterase. *The Plant Cell* 35 (9) , pp. 3544-3565. 10.1093/plcell/koad162

Publishers page: <http://dx.doi.org/10.1093/plcell/koad162>

Please note:

Changes made as a result of publishing processes such as copy-editing, formatting and page numbers may not be reflected in this version. For the definitive version of this publication, please refer to the published source. You are advised to consult the publisher's version if you wish to cite this paper.

This version is being made available in accordance with publisher policies. See <http://orca.cf.ac.uk/policies.html> for usage policies. Copyright and moral rights for publications made available in ORCA are retained by the copyright holders.



# Acetylation of inorganic pyrophosphatase by S-RNase signaling induces pollen tube tip swelling by repressing pectin methylesterase

Chao Tang<sup>1,2,5</sup>, Peng Wang<sup>1,2,5</sup>, Xiaoxuan Zhu<sup>1,2</sup>, Kaijie Qi<sup>1,2</sup>, Zhihua Xie<sup>1,2</sup>, Hao Zhang<sup>1,2</sup>, Xiaoqiang Li<sup>1,2</sup>, Hongru Gao<sup>1,2</sup>, Tingting Gu<sup>1</sup>, Chao Gu<sup>1,2</sup>, Shan Li<sup>1</sup>, Barend H. J. de Graaf<sup>3</sup>, Shaoling Zhang<sup>1,2</sup>, Juyou Wu<sup>1,2,4\*</sup>

<sup>1</sup> Sanya Institute of Nanjing Agricultural University, State Key Laboratory of Crop Genetics & Germplasm Enhancement and Utilization, Nanjing Agricultural University, Nanjing 210095, China

<sup>2</sup> Jiangsu Engineering Research Center for Pear, Nanjing 210014, China

<sup>3</sup> School of Biosciences, Cardiff University, Museum Avenue, Cardiff CF10 3AX, United Kingdom

<sup>4</sup> Jiangsu Key Laboratory for Horticultural Crop Genetic Improvement, Nanjing 210014, China

<sup>5</sup> These authors contributed equally (C.T. and P.W.)

\*Author for correspondence: [juyouwu@njau.edu.cn](mailto:juyouwu@njau.edu.cn) (J.Y.W.)

**Short title:** Tip swelling of SI pollen tubes in pear

The author responsible for distribution of materials integral to the findings presented in this article in accordance with the policy described in the Instructions for Authors (<https://academic.oup.com/plcell/pages/General-Instructions>) is Juyou Wu ([juyouwu@njau.edu.cn](mailto:juyouwu@njau.edu.cn)).

## Abstract

Self-incompatibility (SI) is a widespread genetically determined system in flowering plants that prevents self-fertilization to promote gene flow and limit inbreeding. S-RNase-based SI is characterized by the arrest of pollen tube growth through the pistil. Arrested pollen tubes show disrupted polarized growth and swollen tips, but the underlying molecular mechanism is largely unknown. Here, we demonstrate that the swelling at the tips of incompatible pollen tubes in pear (*Pyrus bretschneideri*, Pbr) is mediated by the SI-induced acetylation of the soluble inorganic pyrophosphatase (PPA). PbrPPA5. Acetylation at Lys-42 of PbrPPA5 by the acetyltransferase GCN5 - related N - acetyltransferase 1 (GNAT1) drives accumulation of PbrPPA5 in the nucleus, where it binds to the transcription factor PbrbZIP77, forming a transcriptional repression complex that inhibits the expression of the pectin methylesterase (PME) gene *PbrPME44*. The function of PbrPPA5 as a transcriptional repressor does not require its pyrophosphatase activity. Downregulating *PbrPME44* resulted in increased levels of methyl esterified pectins in growing pollen tubes, leading to swelling at their tips. These observations suggest a mechanism for PbrPPA5-driven swelling at the tips of pollen tubes during the SI response. The targets of PbrPPA5 include genes encoding cell wall-modifying enzymes, which are essential for building a continuous sustainable mechanical structure for pollen tube growth.

---

## IN A NUTSHELL

**Background:** Self-incompatibility is a widespread genetic mechanism in flowering plants that prevents self-fertilization and promotes outbreeding. S-RNase-based SI is characterized by the arrest of pollen tube growth through the pistil, resulting in disrupted and swollen pollen tube tips that do not reach the ovule and therefore fail to complete fertilization. However, the underlying molecular mechanism responsible for pollen tube tip swelling is still largely unknown.

**Question:** Which factors play roles in pollen tube tip swelling during the self-incompatibility response?

**Findings:** Here we report that the swelling at the tips of incompatible pollen tubes in pear is mediated by self-incompatibility-induced acetylation of the soluble inorganic pyrophosphatase PbrPPA5. Acetylation at Lys-42 of PbrPPA5 by the acetyltransferase PbrGNAT1 caused PbrPPA5 to accumulate in the nucleus. Acetylated PbrPPA5 bound to the transcription factor PbrbZIP77 to form a transcriptional repression complex that inhibited the expression of the pectin methylesterase gene *PbrPME44*. Downregulating *PbrPME44* resulted in increased levels of methyl esterified pectins in growing pollen tubes, leading to swelling at their tips.

**Next steps:** In future studies, we aim to further investigate how the acetyltransferase PbrGNAT1 responds to self-incompatibility signaling and how the soluble inorganic pyrophosphatase PbrPPA5 accumulates in the nucleus.

## Introduction

Self-incompatibility (SI) prevents self-fertilization and promotes outbreeding in a wide range of flowering plant species (de Nettancourt, 2001; Silva and Goring, 2001; Fujii et al., 2016; Zhao et al., 2021b). SI is controlled by a single highly polymorphic locus, the *S* locus, which encodes both male and female *S* determinants. The SI response occurs when the pollen and stigma have the same allele at the *S* locus, for example, during self-fertilization. This causes the arrest of pollen that is genetically identical to the stigma (self pollen) via various mechanisms, ranging from a rapid response that occurs immediately upon pollen germination on the pistil surface to a much slower response that takes place during pollen tube growth through the pistil.

S-RNase-based SI, a major type of self-recognition response that occurs in many flowering plant species, is an example of the slow response in which pollen tube growth through the pistil is arrested (Brugière et al., 2000; Franklin-Tong and Franklin, 2003; Liang et al., 2020; Sun et al., 2022). The female *S* determinants in S-RNase-based SI are pistil-specific glycoproteins that have type T2 ribonuclease activity (Anderson et al., 1986; McClure et al., 1989; McClure et al., 1990). S-RNases from the pistil become internalized by pollen tubes, where they act as cytotoxins that selectively inhibit tube growth in incompatible self pollen (Luu et al., 2000; Goldraij et al., 2006).

---

Pear (*Pyrus bretschneideri*) is a fruit tree species belonging to the Rosaceae family that shows a typical S-RNase-based SI response (Sassa et al., 1992). During SI, S-RNase induces a series of events in the incompatible pollen tube, including depolymerization of the actin cytoskeleton (Liu et al., 2007; Chen et al., 2018), scavenging of tip-localized reactive oxygen species (Wang et al., 2011), swelling at tube tips (Hiratsuka and Tezuka, 1980; Liu et al., 2007), growth arrest (Liu et al., 2007; Chen et al., 2018), and ultimately programmed cell death (Wang et al., 2009; Wang et al., 2011). Swollen tips of pollen tubes are also observed in other species that exhibit S-RNase-based SI, such as sweet tobacco (*Nicotiana glauca*) (Newbigin et al., 1993), petunia (*Petunia inflata*) (Kao and Mccubbin, 1996), passion fruit (*Passiflora edulis*) (Rêgo et al., 2000), and Japanese plum (*Prunus salicina*) (Jia et al., 2008). Disruption of polarized growth of SI pollen tubes ultimately causes their arrest in the pistil, preventing them from reaching the ovary to fertilize the egg cells. However, the molecular mechanism by which S-RNase leads to the swelling of growing pollen tube tips is unknown.

During the delivery of sperm cells into the ovary, the cell wall of the pollen tube provides structural support and protection to prevent overexpansion (Geitmann and Steer, 2006; Parrotta et al., 2019). The cell wall of the pollen tube is composed primarily of cellulose, hemicellulose, and pectin, while the wall at the growing tip mainly consists of pectins. The pectins play a critical role in the delicate regulation of the structural and mechanical properties of polarized pollen tube elongation (Parre and Geitmann, 2005; Zhang et al., 2018) and pollen–pistil interactions (Lu et al., 2019; Duan et al., 2020).

Pectin methyltransferases add methyl substituents to carboxylate groups in homogalacturonan pectins in the Golgi; these pectins are then delivered to the growing pollen tube tip by transport vesicles (Haas et al., 2020). Methyl esters in pectins have low affinity for  $\text{Ca}^{2+}$  and weaken crosslinks in the cell wall (Willats et al., 2001), whereas carboxylate anions that form after de-esterification can form complexes with  $\text{Ca}^{2+}$  and increase cell wall strength (Bosch and Hepler, 2005). During the expansion of pollen tube tips, the methyl ester moieties in pectins are hydrolyzed by tip-secreted pectin methylesterases (PME; EC 3.1.1.11). A gradual decrease in the levels of methyl esterified pectins and an increase in the levels of de-esterified pectins due to localized PME activity are observed at the flanks of pollen tubes (Chebli et al., 2012).

PME activity is important for the elongation and integrity of pollen tubes (Bosch et al., 2005;

---

Tian et al., 2006). In *Arabidopsis* (*Arabidopsis thaliana*), the *PME* mutant *vanguard1* (*vgd1*) shows an uprise in pollen tube tip rupture and reduced male fertility (Jiang et al., 2005). *AtPPME1*, a pollen-expressed *PME* gene in *Arabidopsis*, affects the shape and growth of pollen tubes (Tian et al., 2006).

Many plant species contain large *PME* gene families and express multiple *PME* isoforms in pollen (Bosch and Hepler, 2005; Kim et al., 2020). We recently identified 81 *PME* genes in pear (*PbrPME*), 47 of which are expressed in pollen (Tang et al., 2020b). Knocking down *PbrPME44*, a highly expressed pollen *PME* gene, significantly inhibited pollen tube growth (Tang et al., 2020b). However, the biological function of *PbrPME44* in regulating pollen tube growth and the molecular mechanism of growth arrest, especially during the SI response, are not fully understood. Reduced activities of soluble pyrophosphatases (sPPase, EC 3.6.1.1), which hydrolyze pyrophosphate (PPi) and prevent it from accumulating to toxic levels, result in inhibition of pollen tube growth during the SI response of common poppy (*Papaver rhoeas*) (de Graaf et al., 2006) and apple (*Malus × domestica*) (Li et al., 2018).

In this study, we determined that *PbrPPA5*, a pollen-specific sPPase of pear, is a transcriptional regulator that regulates pollen tube growth and the SI response independently of its sPPase activity. *PbrPPA5* binds to the transcription factor basic LEUCINE ZIPPER 77 (*PbrbZIP77*) and functions as a co-suppressor of *PbrPME44* expression. Following a treatment that mimics the SI response in pollen tubes, *PbrPPA5* was acetylated by GCN5 - related *N* - acetyltransferase 1 (*PbrGNAT1*), thereby promoting its accumulation in the nucleus. The increase in *PbrPPA5* levels in the nucleus reinforced the inhibition of *PbrPME44* expression via the *PbrPPA5*-*PbrbZIP77* complex. The reduction in *PbrPME44* levels in pollen tubes altered the composition and distribution of pectins in the cell wall, resulting in an imbalance between methyl esterified pectins and de-esterified pectins from the tips to the flanks of SI pollen tubes. Thus, our results show that the SI response in pear dramatically alters the mechanical properties of the cell wall and causes swelling at the tips of pollen tubes.

## Results

### SI challenge decreases the expression of *PbrPME44* in pear pollen tubes

To examine the growth of incompatible pollen tubes in vivo, we cross-pollinated (CP; compatible reaction) or self-pollinated (SP; incompatible reaction) pear pistils. At 48 h after pollination, the

---

growth of SP pollen tubes arrested growth halfway through the pistil and the pollen tubes exhibited swelling at the tip, while CP pollen tubes reached the bottom of the pistil (Figure 1A).

We recently developed an *in vitro* pear pollen tube growth system in which adding His-tagged recombinant PbrS-RNases (rPbrS-RNases) to the culture medium mimics the SI response in pollen tubes (Chen et al., 2018), and we refer to this SI-inducing treatment as SI challenge. Following treatment with incompatible rPbrS-RNases (IS), we observed swelling at the tip in pollen tubes (Figure 1B). The frequency of pollen tubes with swollen tips was significantly higher following treatment with IS than with compatible rPbrS-RNases (CS) or a mock treatment. This occurred in a time-dependent manner that was initiated 2 h after IS treatment (Figure 1C, Supplemental Figure S1A and B). Consistently, pollen tubes were significantly shorter following 2 h of IS treatment compared to mock and CS treatments (Supplemental Figure S2).

Because methyl esterified pectins contribute to the swelling at the tips of pollen tubes (Tian et al., 2006; Tang et al., 2020b), we measured the levels of methyl esterified pectins in the apical regions of incompatible pollen tubes. Total pectin contents did not significantly differ among the mock, CS, and IS treatment groups (Supplemental Figure S3). However, the LM20 antibody, which recognizes methyl esterified pectins, detected significant increases in fluorescent signals in the apical region of pollen tubes (the area within 5  $\mu\text{m}$  from the tip to the shank) 2 h after IS treatment (Figure 1D). Fluorescent signals also increased in incompatible pollen tubes without tip swelling, but the increase was lower compared to pollen tubes showing tip swelling (Figure 1E and F, Supplemental Figure S4).

The level of methyl esterified pectins is largely determined by PME activity (Bosch and Hepler, 2005). Total PME enzyme activity decreased in incompatible pollen tubes beginning at 2 h after IS treatment (Supplemental Figure S5). Transcriptome analysis of self-pollinated pistils revealed that five *PbrPME* genes were downregulated during the SI response (Supplemental Figure S6, Supplemental Table S1). Reverse-transcription quantitative PCR (RT-qPCR) analysis of the 47 pollen-expressed *PbrPME* genes (Tang et al., 2020b) revealed that only *PbrPME44* was significantly downregulated (more than two-fold) after IS treatment (Figure 1G, Supplemental Table S2). These results suggest that pistil-expressed *PbrPME* genes are also involved in the SI response in pear. Here, we focus on the function of *PbrPME44*, which is significantly downregulated in incompatible pollen.

---

The expression of *PbrPME44* declined in a time-dependent manner, beginning 2 h after IS treatment (Figure 1H). To confirm the function of *PbrPME44* in the growth of pollen tubes, we performed antisense-oligodeoxynucleotide (as-ODN) inhibition to knock down *PbrPME44* transcript levels. Upon knockdown of *PbrPME44* (Supplemental Figure S7A), the total PME activity in pollen tubes decreased significantly 2 h after as-ODN treatment (Supplemental Figure S7B). Also, the frequency of pollen tubes with swollen tips was higher compared to mock-treated pollen tubes (Supplemental Figure S8A and B). These results are consistent with our previous observation that knocking down *PbrPME44* expression in pear pollen increases the contents of methyl esterified pectins in the apical region of pollen tubes (Tang et al., 2020b). Together, these results suggest that *PbrPME44* affects pollen tube growth in pear.

We tested whether the RNase activity of PbrS-RNase is essential for the repression of *PbrPME44* and the tip swelling of incompatible pollen tubes. An H116R mutation in PbrS-RNases substantially reduces their RNase activity (Chen et al., 2018). The H116R mutant and the wild-type His-Tagged recombinant PbrS-RNases had similar effects on the suppression of *PbrPME44* expression (Figure 1H), the accumulation of methyl esterified pectins (Figure 1D), and the swelling at the tips of pollen tubes (Figure 1C). These results suggest that the RNase activity of PbrS-RNase is not required for suppressing *PbrPME44* expression in incompatible pollen tubes. In addition, the PbrS-RNase<sup>H116R</sup> had similar effects on the inhibition of incompatible pollen tube growth as did the wild-type PbrS-RNase 2 h following the IS treatment (Supplemental Figure S9), indicating that the RNase activity is likely not required in the early stage of SI response.

To explore whether and how *PbrPME44* contributes to the SI response, we added His-tagged recombinant PbrPME44 (rPbrPME44) to the culture medium to compensate for the reduced endogenous PME activity in the SI challenge (Supplemental Figure S10). We treated the pollen tubes with rPbrS-RNases for 2 h, followed by the addition of rPbrPME44 and incubation for an additional 1 h. Pollen tubes contained enlarged knots after IS treatment, whereas their diameters returned to normal and they continued to grow after the addition of rPbrPME44 (Figure 2A). Moreover, the addition of rPbrPME44 reduced the amounts of methyl esterified pectins in IS-treated pollen tubes to levels similar to those observed in mock control and CS-treated pollen tubes (Figure 2A and B).

Using enzyme-linked immunosorbent assays (ELISAs), we observed that the addition of

rPbrPME44 restored the contents of methyl esterified pectins in pollen tubes (Figure 2C and Supplemental Figure S11), and partially alleviated the inhibited growth of pollen tubes induced by SI challenge (Figure 2D). However, if the pollen tubes were treated with incompatible rPbrS-RNase for more than 3 h, the addition of rPbrPME44 failed to restore pollen tube growth (Supplemental Figure S12), suggesting that PbrS-RNase activity reaches a point of no return at 3 h after IS treatment. These results suggest that the downregulation of *PbrPME44* expression plays an important role in the inhibited growth of incompatible pollen tubes rather than representing an effect of the cessation of pollen tube growth.

### **The transcription factor PbrbZIP77 suppresses *PbrPME44* expression**

Using a yeast one-hybrid (Y1H) assay, we investigated the transcriptional regulation of the *PbrPME44* gene using a 1.3-kb promoter sequence upstream of its start codon as a bait to screen a pear cDNA library prepared from total RNA extracted from pollen. We isolated three transcription factors (TFs) (Supplemental Table S3), including a basic leucine zipper (bZIP) TF (Figure 3A; Pbr031203.1; named PbrbZIP77; Ma et al., 2021). PbrbZIP77 shares 55.9% amino acid sequence identity with Arabidopsis AtbZIP34 (At2g42380) (Supplemental Figure S13A), Mutations in *AtbZIP34* cause morphological defects in the pollen grain wall (Gibalová et al., 2009). RT-PCR analysis of pear tissues showed that *PbrbZIP77* was expressed in pollen tubes (Supplemental Figure S13B), supporting its role in pollen tube growth.

Analysis of the regulatory *cis*-elements in the *PbrPME44* promoter fragment identified two potential bZIP binding sites: an abscisic acid–responsive element (ABRE) at position –1,192 to –1,187 and a C-box element at position –139 to –134 (Figure 3A; Supplemental Data Set S1). To determine whether PbrbZIP77 binds one or both of these *cis*-elements, we introduced mutations at these sites and performed another Y1H analysis. The ACATGG to ACCCCG mutation in the ABRE motif blocked the interaction between the *PbrPME44* promoter and PbrbZIP77, whereas the CACGTC to CCCCCC mutation in the putative C-box did not (Figure 3A).

To further explore the interaction between PbrbZIP77 and a 30-bp promoter fragment containing the putative ABRE binding site, we performed electrophoretic mobility shift assays (EMSAs) and bio-layer interferometry (BLI) assays. In the EMSA, recombinant His-PbrbZIP77 specifically bound to the biotin-labeled ABRE fragment, and this specific binding was reduced by competition with cold probe included at a five-fold higher concentration, but not affected by the ABRE mutated probe

---

(Figure 3B). Quantification of the interaction using BLI showed that the binding affinity ( $K_d$ ) between His-PbrbZIP77 and the ABRE fragment was  $6.3 \pm 1.5 \mu\text{M}$  (Figure 3C).

To better understand the function of PbrbZIP77 in *PbrPME44* expression, we performed dual-luciferase reporter assays. PbrbZIP77 decreased firefly luciferase (LUC) activity derived from the *PbrPME44pro:LUC* reporter construct, but it had no significant effect on activity from *PbrPME44-(ABREmut)pro:LUC* (Figure 3D). In pollen tubes containing a *PbrbZIP77*-knockdown generated using as-ODN (Supplemental Figure S14A), we detected a significant increase in *PbrPME44* expression (Figure 3E). This was accompanied by higher total PME activity (Figure 3F) and lower levels of methyl esterified pectins (Figure 3G). In addition, *PbrbZIP77*-knockdown pollen tubes were significantly shorter than the those of the mock control (Supplemental Figure S14B). These results suggest that PbrbZIP77 in the pollen binds to the ABRE *cis* element of the *PbrPME44* promoter, resulting in the suppression of *PbrPME44* transcription.

#### **PbrPPA5 physically interacts with PbrbZIP77**

Upon SI challenge, the expression level of *PbrbZIP77* was not affected in pear pollen tubes (Supplemental Figure S15), suggesting that other regulators might be involved in SI. In a yeast two-hybrid (Y2H) screen, we identified 17 candidate interacting proteins of PbrbZIP77 that are encoded by genes expressed in pollen (Supplemental Table S4). One of these candidates was the soluble inorganic pyrophosphatase (sPPase; Pbr025893.1) PbrPPA5 (Tang et al., 2020a). Five *PbrPPA* genes are expressed in pear pollen, but only *PbrPPA5* is specifically expressed in pollen (Tang et al., 2020a). Y2H assays showed that only PbrPPA5 interacted with PbrbZIP77 (Figure 4A; Supplemental Figure S16). We confirmed the interaction between PbrbZIP77 and PbrPPA5 *in planta* by bimolecular fluorescence complementation (BiFC) and luciferase complementation imaging (LCI) assays (Figures 4B and C). In addition, microscale thermophoresis (MST) analysis showed that the binding affinity ( $K_d$ ) between PbrPPA5-His and PbrbZIP77-His was  $27.5 \pm 4.2 \text{ nM}$  (Figure 4D).

The pyrophosphatase activity of sPPase catalyzes the hydrolysis of PPi to inorganic phosphate (Pi). To examine whether PbrPPA5 has sPPase activity, we produced and purified His-tagged recombinant PbrPPA5 (rPbrPPA5) from *Escherichia coli* (Supplemental Figure S17A). The sPPase activity of rPbrPPA5 ( $220.80 \pm 12.43 \mu\text{mol Pi mg}^{-1} \text{ min}^{-1}$ ; Supplemental Figure 17B) was very similar to that of other plant sPPases, including those of poppy and apple pollen (de Graaf et al., 2006; Li

---

et al., 2018). In addition, PbrPPA5 shares 68.55% amino acid sequence similarity with Prp26.1a/b, the sPPases identified in common poppy (Supplemental Figure S17C). These results confirm the notion that PbrPPA5 is a classical sPPase.

We asked whether the interaction between PbrbZIP77 and PbrPPA5 requires the intrinsic pyrophosphatase activity of PbrPPA5. The DxDPxDV motif, which is highly conserved in plant PPase enzymes, is part of the Mg<sup>2+</sup>-binding site and is essential for pyrophosphatase activity (de Graaf et al., 2006; Grzechowiak et al., 2019). Indeed, we identified a DxDPxDV motif in PbrPPA5 (position 134–140, DNDPLDV). We mutated D136 to Asn (N) and P137 to Ala (A) and observed that these mutant sPPases had significantly reduced pyrophosphatase activity (Supplemental Figure S18A). However, these mutant PbrPPA5s still interacted with PbrbZIP77 in a Y2H assay (Supplemental Figure S18B). We demonstrated that the segment of PbrPPA5 at positions 214–234, which is less conserved among sPPases, is responsible for the interaction with PbrbZIP77 in Y2H assays (Supplemental Figure S18C). These results suggest that the intrinsic pyrophosphatase activity of PbrPPA5 is not required for its interaction with PbrbZIP77.

#### **PbrPPA5 acts with PbrbZIP77 to co-suppress *PbrPME44* expression**

We investigated whether PbrPPA5 is involved in the transcriptional regulation of *PbrPME44* in growing pear pollen tubes. Knockdown of *PbrPPA5* using as-ODN (Supplemental Figure S19A) resulted in the significant upregulation of *PbrPME44* expression (Supplemental Figure S19B). Accordingly, relative PME activity was higher in *PbrPPA5*-knockdown pollen tubes than in the wild-type pollen tubes (Supplemental Figure S19C), and the levels of methyl esterified pectins were dramatically reduced at the tips of pollen tubes of these plants (Supplemental Figure S19D and E). In dual-luciferase assays, PbrPPA5 alone failed to modify the activity of the *PbrPME44* promoter; however, when *PbrPPA5* and *PbrbZIP77* were co-expressed, *PbrPME44* expression was significantly reduced (Figure 5A). In EMSAs, the addition of PbrPPA5 together with His-PbrbZIP77 resulted in the appearance of a super-shifted complex on the ABRE site from *PbrPME44* promoter. Notably, this complex had a stronger intensity than seen with His-PbrbZIP77 alone, suggesting that the binding of His-PbrbZIP77 to the ABRE was enhanced by adding higher concentrations of His-PbrPPA5 (Figure 3B). In addition, the suppression of *PbrPME44* expression was not affected when the sPPase domain of PbrPPA5 was mutated (D136N or P137A) (Figure 5B). These results suggest

---

that the presence of PbrPPA5 enhances the suppression of *PbrPME44* expression by PbrbZIP77.

### SI-induced acetylation of PbrPPA5 causes it to accumulate in the nucleus

Although a direct interaction between S-RNases and sPPases in SI responses has been reported in apple (Li et al., 2018), we did not observe a direct interaction between PbrS-RNase and PbrPPA5 in our Y2H assays (Supplemental Figure S20). During the SI response in poppy, the sPPases Prp26.1a/b are rapidly phosphorylated, resulting in a decrease in sPPase activity in pollen (de Graaf et al., 2006; Eaves et al., 2017). However, after 2.5 h of SI challenge, we detected neither a decrease in total sPPase activity nor the phosphorylation of PbrPPA5 in pollen tubes (Supplemental Figure S21). Notably, we detected acetylation at the Lys-42 (K42) residue (LMASEDQSEEAK) of PbrPPA5 by mass spectrometry of proteins extracted from pollen tubes 1.5 h after SI challenge (Supplemental Figure S22; Supplemental Data Set S2).

The acetylation of proteins can alter their localizations and functions (Drazic et al., 2016). The substitution of a basic, positively charged Lys residue for an uncharged glutamine (Q) or a charge-conservative arginine (R) can mimic a constitutively acetylated or non-acetylated status, respectively (Kim et al., 2006). We therefore generated *PbrPPA5*<sup>K42Q</sup> (constitutively acetylated) and *PbrPPA5*<sup>K42R</sup> (non-acetylated) mutant constructs and fused them to *GFP* (green fluorescent protein) to study the effect of acetylation of the K42 residue on the localization of PbrPPA5. Following transient expression in epidermal leaf cells of *Nicotiana benthamiana*, the K42Q mutation increased the nuclear localization of PbrPPA5, whereas the K42R mutation reduced its nuclear localization (Figure 6A-D). Consistently, when we used particle bombardment to deliver constructs expressing the mutant proteins with K42Q as an acetylation mimic into pollen tubes, the K42Q mutation increased the nuclear localization of PbrPPA5 in the nucleus and led to swelling at the tips of pollen tubes (Figure 6E and F, Supplemental Figure S23).

In addition, acetylation of the K42 residue did not affect the pyrophosphatase activity of PbrPPA5 (Supplemental Figure S24), the interaction between PbrPPA5 and PbrbZIP77 (Supplemental Figure S25), or the co-suppressor activities of PbrPPA5 for *PbrPME44* (Supplemental Figure S26). We noted that two other lysine residues of PbrPPA5, K9 and K98, could be acetylated as well. However, mutating either K9 (Supplemental Figure S27A–C) or K98 (Supplemental Figure S27D–F) had no visible effect on PbrPPA5 localization, suggesting that these two lysine residues are not associated with SI. These results indicate that acetylation of the K42

---

residue in PbrPPA5 promotes its accumulation in the plant cell nucleus.

To identify the acetyltransferase responsible for the acetylation of PbrPPA5 during SI, we used a cDNA library generated from pear pollen to perform a Y2H assay to screen for proteins interacting with PbrPPA5. One interacting protein was a GCN5 - related *N* - acetyltransferase (Pbr013581.1; named PbrGNAT1, Figure 7A). In BiFC assays, PbrGNAT1 interacted with PbrPPA5 in both the nucleus and the cytoplasm (Figure 7B). In acetylation activity assays, PbrGNAT1 induced the acetylation of PbrPPA5, which was dependent on the K42 residue (Figure 7C). PbrPPA5 accumulated in the nucleus more frequently when PbrGNAT1 was presented (Figure 7D, E and F). In addition, the *PbrGNAT1* transcript level increased at 1 h after IS treatment, supporting the notion that PbrGNAT1 is involved in the SI response in pear (Figure 7G).

Finally, because SI caused the acetylation of the K42 residue of PbrPPA5, we investigated whether PbrPPA5 accumulated in the nuclei of incompatible pollen tubes. PbrPPA5 was significantly more abundant in the nuclei of pollen tubes after IS treatment, as revealed by immunoblot analysis of cellular fractions (Figure 8A). When *PbrPPA5-GFP* was transiently expressed in pear pollen tubes via particle bombardment, PbrPPA5-GFP was enriched in the generative nucleus of SI pollen tube 1.5 h after SI challenge (Figure 8B and C, Supplemental Figure S28). These results suggest that SI induces the nuclear accumulation of PbrPPA5 in pear pollen tubes.

## Discussion

The swelling at the tips of pollen tubes during S-RNase-based SI has been observed for over 40 years (Hiratsuka and Tezuka, 1980; Liu et al., 2007), but the underlying molecular mechanisms are still largely unknown. Here, we identified a signaling pathway that led to the repression of *PbrPME44* expression and altered the structural composition of pectins in the cell walls of growing pollen tubes during the SI response (Figure 9). Under SI challenge, *PbrGNAT1* was upregulated within 1 h, leading to the acetylation of PbrPPA5 in 1.5 h. In turn, the acetylation of PbrPPA5 promoted its accumulation in the nuclei of pollen tubes, where PbrPPA5 bound to PbrbZIP77 and together co-suppressed *PbrPME44* expression. Moreover, the role of PbrPPA5 as a co-suppressor of *PbrPME44* expression was independent of its sPPase activity. The reduction in PbrPME44 levels disturbed the balance between methyl esterified and de-esterified pectin at growing pollen tube tips after SI challenge, disrupting polarized growth and leading to swelling at the tips of pollen tubes.

---

## PbrPME44 mediates tip swelling of pollen tubes following SI challenge

Maintaining the biomechanical equilibrium and stability of different cell wall components in the pollen tube tip is essential for the polarized growth of pollen tubes (Bosch and Hepler, 2005). Methyl esterified and de-esterified pectins are major components of the cell wall whose abundance and ratio play critical roles in determining the shape and integrity of growing pollen tubes (Duan et al., 2020; Zhou et al., 2021). SI-induced tip swelling of pear pollen tubes is not related to changes in total pectin content (Supplemental Figure S3) but is associated with increased levels of methyl esterified pectins (Figure 1). This increase may result in the softening of the pollen tube tip wall (Bosch and Hepler, 2005). It should be noted that the tips of most incompatible pollen tubes do not swell, possibly due to insufficient accumulation of methyl esterified pectin (Figure 1). Meanwhile, we could not exclude the possibility that some other factors participate in the growth arrest of incompatible pollen tubes in SI response of pear.

Our results uncover the relationship among growth arrest, tip swelling, and methyl esterification of pectin at the apical regions of incompatible pollen tubes in pear. During the early stage following the SI challenge, PbrPME44 restored the level of methyl esterified pectins and the growth of pollen tubes (Figure 2). Therefore, downregulating *PbrPME44* leads to insufficient PME activity, which affects the methyl esterification of pectin in pollen tubes and contributes to tip swelling.

We propose a holding phase during the SI response in which the pollen tube remains plastic to provide another fertilization opportunity for the arrested pollen tube when the SI conditions weaken for one reason or another (Cheung, 2022). For example, SI-induced ATP depletion has been suggested to be the holding phase before programmed cell death of pollen tubes during the SI response in common poppy (Wang et al., 2022). Thus, the tip swelling of incompatible pollen tubes could be a holding phase in the SI response of pear. During later stages of the SI challenge, pollen tube growth failed to be restored by PbrPME44 (Supplemental Figure S12), suggesting that the cessation of growth of incompatible pollen tubes might be determined by other factors, such as actin depolymerization (Chen et al., 2018).

The RNase activity of PbrS-RNase was not required for the downregulation of PbrPME44 (Figure 1). Combined with results showing S-RNase-mediated actin disruption in apple and pear (Chen et al., 2018; Yang et al., 2018; Zhao et al., 2021a), and heat-inactivated S-RNase exerting a more severe inhibition of pollen tubes in *N. alata* (Gray et al., 1991), we suggest that PbrS-RNase

---

could also function in signaling pathways independent of its enzymatic activity in the SI response.

### **The PbrbZIP77-PbrPPA5 complex suppresses the expression of *PbrPME44***

In Arabidopsis, AtbZIP34 regulates *PME* gene expression and pollen wall development (Gibalová et al., 2009). We demonstrated that PbrbZIP77, a homolog of AtbZIP34, bound to the promoter region of *PbrPME44* and inhibited its expression (Figure 3). We also identified PbrPPA5a as an interacting partner of PbrbZIP77. PbrPPA5 is a classic Mg<sup>2+</sup>-dependent sPPase; these proteins localize to the nucleus and cytoplasm. Two functions of sPPases in the nucleus have been proposed: 1) sPPases are essential for hydrolysis of PPi, as during nucleic acid biosynthesis in Arabidopsis (Segami et al., 2018); and 2) sPPases are important for nucleosome remodeling in *Drosophila melanogaster* (Gdula et al., 1998). Our results propose a role for an sPPase in transcriptional regulation. PbrPPA5 interacted directly with PbrbZIP77 and enhanced PbrbZIP77-mediated transcriptional repression of *PbrPME44*, whereas PbrPPA5 alone did not inhibit *PbrPME44* expression. Moreover, the downregulation of *PbrPME44* expression by the PbrPPA5–PbrbZIP77 transcriptional complex was independent of the intrinsic pyrophosphatase activity of PbrPPA5, suggesting that PbrPPA5 functions as a transcriptional regulator in pear pollen (Figure 5).

### **Acetylation of PbrPPA5 promotes its accumulation in nuclei during SI**

The roles of sPPases in SI signaling have been reported in poppy and apple. During the Ca<sup>2+</sup>-mediated SI response in poppy, two sPPases, Prp26.1a and 1b, become phosphorylated, significantly reducing their sPPase activity (de Graaf et al., 2006; Eaves et al., 2017). By contrast, MdPPa in apple pollen is not phosphorylated during the SI response; rather, the S-RNase responsible for the SI response in apple interacts with MdPPa in pollen and inhibits its enzymatic activity (Li et al., 2018). Unlike in apple and poppy, we established that PbrPPA5 in pear was not phosphorylated and did not interact with PbrS-RNases upon SI challenge. The SI mechanisms for pollen tube growth inhibition are differentially regulated (temporally and spatially) in pear compared to poppy. In pear, the SI response is slow; the female determinants PbrS-RNases enter the growing pollen tubes via endocytosis or an unknown mechanism, after which they exert their toxic effects (Liu et al., 2007; Chen et al., 2018). In poppy, the female determinant PrsS does not enter the cytoplasm of pollen, instead acting as a ligand by interacting with its cognate membrane-localized pollen receptor-like determinant PrpS to induce a series of signaling events in the pollen cytosol,

---

triggering a rapid SI response characterized by inhibited pollen germination and tube growth (Thomas and Franklin-Tong, 2004; Bosch and Franklin-Tong, 2007; Wheeler et al., 2009; Wang et al., 2018; Lin et al., 2022).

We determined that PbrPPA5 became acetylated after the SI challenge (Supplemental Figure S22 and Supplemental Data Set S2), and posttranslational modifications such as this can alter the localization of a protein (Wang et al., 2010; Baeza et al., 2016; Narita et al., 2019; Zhu et al., 2019). In healthy growing pollen tubes, PbrPPA5 localizes to both the cytoplasm and nuclei. Under SI challenge, the K42 residue of PbrPPA5 was acetylated by PbrGNAT1, leading to the more frequent nuclear accumulation of this modified PbrPPA5 (Figure 8). The nuclear accumulation of PbrPPA5 could result from an increase in its import rate, a decrease in its export rate, or a sequestration mechanism in which formation of a complex with other nuclear proteins increases its residence time inside the nucleus. Further investigation is needed to determine the underlying mechanism.

In conclusion, we present a model describing how the acetylation of PbrPPA5 elicits the swelling of pollen tube tips following SI challenge in pear (Figure 9). In healthy growing pollen tubes, PbrbZIP77 suppresses the expression of *PbrPME44* to maintain the balance between methyl esterified and de-esterified pectin levels at the expanding pollen tube tip. During the SI response, *PbrGNAT1* is upregulated, and PbrGNAT1 acetylates PbrPPA5, promoting its nuclear accumulation. Nucleus-localized PbrPPA5 binds to PbrbZIP77, forming a complex that suppresses *PbrPME44* expression. Downregulation of *PbrPME44* leads to higher levels of methyl esterified pectin, thus decreasing cell wall rigidity and ultimately resulting in the swelling of pollen tube tips. Overall, our elucidation of the role of PbrPPA5 in SI opens avenues for studying S-RNase-based SI. In addition, our findings shed light on the important role of the PbrPPA5–PbrbZIP77 complex in gene regulation as it fine-tunes the production of one plant cell wall-modifying enzyme in order to build a continuous sustainable mechanical structure for plant cell development.

## Materials and Methods

### Plant materials

Pollen from *Pyrus bretschneideri* cv. Dangshansuli (S<sub>7</sub>S<sub>34</sub>) was collected from specimens growing at the Nanjing Agricultural Fruit Experimental Yard, China. After drying for 24 h at room temperature, the mature pollen was stored in silica gel at –20°C for the subsequent experiments. Roots, stems,

---

leaves, and fruits were collected and frozen immediately in liquid nitrogen and stored at  $-80^{\circ}\text{C}$ . Pistils were isolated and transferred into storage tubes and kept in liquid nitrogen until use.

### **Aniline blue staining of pollen tubes in pistils**

Aniline blue staining was performed as previously described with some modification (Hiratsuka and Tezuka, 1980). The pre-emasculated mature flowers of Dangshansuli ( $S_7S_{34}$ ) were pollinated with either Dangshansuli ( $S_7S_{34}$ , self-pollination) or Huanghua ( $S_1S_2$ , cross-pollination) pollen. The pistils were collected 48 h after pollination and fixed in ethanol:acetic acid (3:1 v/v) for at least 2 h at room temperature. The fixed pistils were washed with 70%, 50%, and 30% ethanol for 10 min each, then washed with distilled water for 10 min and finally softened overnight in a solution of 2 M NaOH. The softened pistils were washed three times with distilled water and stained overnight in aniline blue solution (0.1% w/v aniline blue in 0.1 M  $\text{K}_3\text{PO}_4$  buffer, pH 7.3) at  $37^{\circ}\text{C}$  in the dark. The stained pistils were observed using an IX73 fluorescent microscope (Olympus, Japan).

### **Pollen culture, measurement, and S-RNase treatments**

Pollen was cultured in liquid germination medium (0.5 mM  $\text{Ca}(\text{NO}_3)_2$ , 1.5 mM  $\text{H}_3\text{BO}_3$ , 450 mM sucrose, and 25 mM 2-(*N*-morpholino) ethanesulfonic acid hydrate (MES), pH 6.0–6.5). Pollen tube diameters and lengths were measured under a light microscope using ImageJ software (<https://imagej.nih.gov/ij/>).

His-tagged recombinant PbrS-RNase (rPbrS-RNase) proteins were produced by according to a previously described method (Chen et al., 2018). For IS treatments, pollen tubes (Dangshansuli;  $S_7$  or  $S_{34}$ ) were pre-cultured in liquid germination medium for 1.5 h and treated with rPbr $S_7$ -RNase plus rPbr $S_{34}$ -RNase protein (at a final concentration of 0.15 U) or the same amount of mutant rPbr $S_7$ -RNase<sup>H116R</sup> plus rPbr $S_{34}$ -RNase<sup>H116R</sup> (H116R) protein added to the pollen cultures in vitro. For CS treatments, pollen tubes (Dangshansuli;  $S_7$  or  $S_{34}$ ) were pre-cultured for 1.5 h after which rPbr $S_1$ -RNase and rPbr $S_2$ -RNase were added. For PME compensation experiments, pollen tubes were pre-cultured for 1.5 h and treated with rPbr $S_7$ -RNase plus rPbr $S_{34}$ -RNase proteins or rPbr $S_7$ -RNase<sup>H116R</sup> plus rPbr $S_{34}$ -RNase<sup>H116R</sup> proteins for another 2.0 h or 3.0 h, then 0.005 mg  $\text{mL}^{-1}$  His-tagged recombinant PbrPME44 (rPbrPME44) proteins were added, respectively, and treated for 1.0 h.

### **Illumina sequencing and analysis of transcriptome data**

---

At 48 h and 72 h after pollination, self-pollinated and cross-pollinated pistils were collected, immediately frozen in liquid nitrogen, and stored at  $-80^{\circ}\text{C}$ . Total RNA was extracted from the frozen tissue mentioned above using a Plant Total RNA Isolation Kit (Foregene, China) according to the manufacturer's instructions. mRNA samples were extracted from total RNA using the VAHTS mRNA-SEQ V2 Library Prep Kit (Vazyme, China) according to the manufacturer's instructions. Double-stranded cDNA was reverse-transcribed and amplified by Illumina gene expression sample preparation kit (Illumina, USA). An Illumina Novaseq 6000 instrument was used to perform the sequencing reactions. Clean reads were obtained by FASTP software (<https://github.com/OpenGene/fastp>). Hisat2 (<http://daehwankimlab.github.io/hisat2/>) was used to align clean reads to the reference genome of pear v1.0 (<http://www.peargenome.njau.edu.cn>). Gene expression levels were calculated based on raw counts and were normalized using DESeq2 (Love et al., 2014). Finally, all differentially expressed genes were annotated using the Kyoto Encyclopedia of Genes and Genomes (KEGG; <http://www.genome.jp/kegg/>).

### **Immunohistochemical analysis of pollen tubes**

The immunohistochemical analysis of methyl esterified pectins in pollen tubes was performed as previously described (Wang et al., 2017). The primary antibodies used in our study were Leeds Monoclonal 20 (LM20, University of Leeds, UK; <http://www.plantprobes.net/>), which labels methyl esterified homogalacturonan (HG) (1:20 dilution). Anti-rat IgG-fluorescein isothiocyanate-conjugated (FITC) antibody (1:500 dilution; F1763, Sigma-Aldrich, USA) was used as the secondary antibody. The fluorescence was imaged using a LSM800 confocal microscope with Airyscan (Carl Zeiss, Germany) and quantified using ZEN imaging software (Carl Zeiss, Germany). The excitation wavelength and transmission range for emission were 488 nm/500-550 nm for the FITC channel, and the detector gain was 700 V.

### **Analysis of methyl esterified HG in the pollen tube cell wall using ELISA**

The alcohol-insoluble residue of the pollen tube cell wall was generated as previously described (Silva-Sanzana et al., 2019), and its components were sequentially extracted with 2 mL water and *trans*-1,2-diaminocyclohexane-N,N,N',N'-tetraacetic acid (CDTA) to generate soluble fractions containing HG (Wang et al., 2019). ELISA was performed as described previously (Willats et al.,

---

1998). A primary HG-directed antibody (LM20) was used as a 10-fold dilution, and the horseradish peroxidase (HRP)-conjugated goat anti-rabbit IgG antibody that was used as the secondary antibody (Sangon, China) was added at a 1000-fold dilution. The absorbance of each well at 450 nm was determined using a CYTATION3 microplate reader (BioTek, USA). At least three independent experiments were performed.

### Measurement of total pectins

After 2.0 h mock, SC and SI treatments, pollen samples were collected by centrifuging at 13,500 *g* and ground in liquid nitrogen. After the addition of 1 mL 95% ethyl alcohol, pollen samples were incubated in a water bath at 80°C for 30 min. They were then centrifuged at 13,500 *g* for 2 min before being sequentially washed with 2 mL 85% ethyl alcohol, 2 mL methyl alcohol: chloroform (1:1), and 2 mL acetone. Samples containing the resulting sediments were left to dry by evaporation at room temperature overnight. Total pectins were measured using a Total Pectin Content Test Kit (Solarbio, China). The absorbance of each well at 530 nm was determined using a CYTATION3 microplate reader (BioTek, USA). At least three independent experiments were performed.

### Reverse-transcription PCR (RT-PCR) analysis

RT-PCR analysis was performed to confirm the presence of *PbrbZIP77* transcripts in the pollen tubes, pistils, roots, stems, leaves, and fruits. Total RNA was extracted from the samples mentioned above, then reverse-transcribed using the RevertAid RT Reverse Transcription Kit (Thermo Fisher Scientific, USA), according to the manufacturer's instructions.

The reaction mixture for RT-PCR contained 0.1  $\mu$ L cDNA, 4  $\mu$ L 0.1  $\mu$ M gene-specific primer mixture, 10  $\mu$ L 2 $\times$ Taq Plus Master Mix (Vazyme, China), and 5.9  $\mu$ L double-distilled water in a total volume of 20  $\mu$ L. PCR was performed with the following program: 3 min at 94°C; 25 cycles of 30 s at 94°C, 30 s at 60°C, and 30 s at 72°C; and a final 10-min extension at 72°C. The *PbrTUB-2* (XP\_009374320.1) was used as the reference gene. PCR products were fractionated in 2% agarose gels. Primers are listed in Supplemental Data Set S3.

### RT-qPCR

The expression levels of *PbrbZIP77* and 47 *PbrPME* under mock, SI, and SC treatments were

quantified using quantitative real-time PCR (qPCR). The qPCR reaction mixture contained 0.2  $\mu$ L cDNA sample, 5  $\mu$ L 0.5  $\mu$ M gene-specific primer mixture, 10  $\mu$ L 2 $\times$ SYBR Green Master Mix, and 4.8  $\mu$ L water in a total volume of 20  $\mu$ L. qPCR was performed using the LightCycler SYBR Green I Master (Roche, Germany). Relative expression levels were calculated using the  $2^{-\Delta\Delta CT}$  method (Livak and Schmittgen, 2001), with *PbrTUB-2* as the internal standard. A melting curve was performed to verify the specificity of all qPCR primers. At least three biological replicates were employed for each experiment. The heat map was generated using TBtools (Chen et al., 2020). The primers are listed in Supplemental Data Set S3.

### Point mutants and Y1H assay using the *PbrPME44* promoter

The 1.3-kbp promoter sequence of *PbrPME44* was amplified from pear genomic DNA using PCR and then cloned into the pAbAi vector (Clontech, USA) to use as bait for screening the Dangshansuli pollen cDNA library. Y1H assays were performed using the Matchmaker Gold Yeast One-Hybrid Library Screening System (Clontech, USA).

For the interaction assays, the DNA elements were analyzed using PlantCARE (<http://bioinformatics.psb.ugent.be/webtools/plantcare/html/>). Point mutations (ABRE mut, C-box mut) were introduced using a Fast Mutagenesis System (Transgen, China). Promoters used for the Y1H assay were cloned into pAbAi to generate *PbrPME44pro:pAbAi*, *PbrPME44(ABREmut)pro:pAbAi*, and *PbrPME44(C-box mut)pro:pAbAi* plasmids, which were integrated into the Y1HGold yeast strain as bait. Full-length *PbrbZIP77* cDNA was fused into the pGADT7 AD vector (Clontech, USA) to generate PbrbZIP-AD, which was introduced into the three bait strains. p53-pAbAi and AD-Rec53 (Clontech, USA) were introduced into the Y1HGold strain as a positive control. The co-transformed yeast cells were cultured on SD (Synthetic Dropout)/–Leu plates (Clontech, USA) with or without aureobasidin A (AbA) (400 ng mL<sup>-1</sup>) and incubated at 30°C for 3 d.

### Expression and purification of recombinant proteins

Full-length cDNAs of *PbrS<sub>1/2/7/34</sub>-RNase* (without the signal peptide sequence), *PbrS<sub>7/34</sub>-RNase<sup>H116R</sup>* (without the signal peptide sequence), *PbrPPA5*, *PbrPPA5<sup>K42Q</sup>*, *PbrPPA5<sup>K42R</sup>*, *PbrPPA5<sup>D136N</sup>*, *PbrPPA5<sup>P137A</sup>*, *PbrbZIP77*, and *PbrPME44* (without the N-terminal hydrophobic motif) were amplified

by PCR and individually inserted into pCold-TF vectors (Takara, Japan). pCold-TF is a fusion cold shock expression vector that expresses trigger factor chaperone as a soluble tag. Trigger factor is a prokaryotic ribosome-associated chaperone protein (48 kDa) that facilitates co-translational folding of newly expressed polypeptides. Primers are listed in Supplemental Data Set S3. The rPbrS<sub>1/2/7/34</sub>-RNase, rPbrS<sub>7/34</sub>-RNase<sup>H116R</sup>, His-tagged recombinant PbrPPA5 (rPbrPPA5), His-tagged recombinant PbrPPA5<sup>K42Q</sup> (rPbrPPA5<sup>K42Q</sup>), His-tagged recombinant PbrPPA5<sup>K42R</sup> (rPbrPPA5<sup>K42R</sup>), His-tagged recombinant PbrPPA5<sup>D136N</sup> (rPbrPPA5<sup>D136N</sup>), His-tagged recombinant PbrPPA5<sup>P137A</sup> (rPbrPPA5<sup>P137A</sup>), His-tagged recombinant PbrbZIP77 (rPbrbZIP77), and rPbrPME44 were expressed as fusion proteins in *E. coli* strain BL21 Rosetta (DE3) (Transgen, China). A 10-mL liquid culture of recombinant *E. coli* protein was incubated overnight at 37°C in the presence of ampicillin (0.1 mg/mL) and transferred to fresh LB (Luria-Bertani) medium as a 1:50 dilution (10 mL overnight culture added to 490 mL LB medium). The cultures were grown at 37°C for another 1–4 h. When OD<sub>600</sub> of the suspension reached 0.4–0.6, the suspension was rapidly cooled to a 15°C and incubated for 30 min at 15°C. After this, 0.5 mM IPTG was added and the culture was shaken at 15°C for 24 h to induce protein expression in the cells, which were then harvested by centrifugation at 13,500 *g* and stored at –20°C until required for protein extraction.

For protein extraction, cells were resuspended in 30 mL lysis buffer (50 mM Tris-HCl, 140 mM NaCl, 2 mM EDTA, and 5 mM imidazole, pH 7.9) supplemented with cOmplete EDTA-free protease inhibitor cocktail (Roche, Germany) and vigorously mixed. The suspension was sonicated five times on ice for 7 s each time, with a 20-s rest between each pulse to allow cooling. The lysate was centrifuged (13,500 *g*, 15 min) at 4°C, after which the supernatant was recovered and filtered through a 0.45- $\mu$ m pore size filter membrane (MilliporeSigma, USA). For rPbrPPA5, rPbrPPA5<sup>K42Q</sup>, rPbrPPA5<sup>K42R</sup>, rPbrPPA5<sup>D136N</sup>, and rPbrPPA5<sup>P137A</sup>, the supernatant containing the soluble protein was loaded onto a column containing 2 mL NTA-Ni<sup>+</sup> His Bind resin in phosphate buffered saline (PBS) (MilliporeSigma, USA) and washed with 20 mL binding buffer (500 mM NaCl, 5 mM imidazole, and 20 mM Tris-HCl, pH 7.9), then 40 mL wash buffer (500 mM NaCl, 30 mM imidazole, and 20 mM Tris-HCl, pH 7.9) prior to being eluted with 6 mL elution buffer (500 mM NaCl, 50 mM imidazole, and 20 mM Tris-HCl, pH 7.9). For rPbrbZIP77, the wash buffer was changed to 500 mM NaCl, 50 mM imidazole, and 20 mM Tris-HCl (pH 7.9), and the elution buffer was 500 mM NaCl, 90 mM imidazole, and 20 mM Tris-HCl (pH 7.9). For rPbrPME44, the elution buffer was 500 mM NaCl, 60 mM

---

imidazole, and 20 mM Tris-HCl (pH 7.9). The rPbrS-RNases were produced as described previously (Chen et al., 2018). Fractions were desalted and concentrated by centrifugal ultrafiltration (6,000 g, 5 min) using 30 kDa Amicon Ultra-4 tubes (MilliporeSigma, USA) and equilibrated with 25 mM Tris-HCl (pH 8.0), PBS or liquid germination medium.

## EMSA

An EMSA was performed using the LightShift Chemiluminescent EMSA Kit (Thermo Fisher Scientific, USA), according to the manufacturer's protocol. The rPbrbZIP77 and rPbrPPA5 were produced as described above. An oligonucleotide probe (with or without a biotin label) representing the ABRE motif was synthesized by Genewiz (Suzhou, China). The binding activity of rPbrbZIP77 was analyzed using the sequence containing the ABRE motif and its flanking sequence, and additional rPbrPPA5 was added to detect the super-shift band. The sequences of the oligonucleotide probes are listed in Supplemental Data Set S3.

## BLI assay

The binding affinities of rPbrbZIP77 and the ABRE probe were assessed using an Octet RED96 (FortéBio, USA) equipped with a streptavidin (SA) sensor (Pall, USA). Water was used as a negative control. The experiments were conducted at room temperature in water containing 0.02% Tween-20. The SA sensor tips were immersed into wells containing different concentrations of rPbrbZIP77 (342 nM, 384 nM, 427 nM, 570 nM, 712 nM, and 855 nM). The biotin-labeled oligonucleotide probe of the ABRE motif was synthesized by Genewiz (Suzhou, China). Double stranded ABRE primers (0.1  $\mu$ M) were produced by annealing and loaded onto SA biosensors until saturation. Each data set was fitted globally to a 1:1 interaction model (FortéBio, USA) to determine the kinetic parameters,  $k_{on}$  and  $k_{off}$ . The apparent affinities were then calculated as a ratio ( $k_{off}/k_{on}$ ) of these rate constants using Data Analysis software v9.0.0.14 (FortéBio, USA). The sequences of the oligonucleotide probes are listed in Supplemental Data Set S3.

## Dual-luciferase reporter assay

The full-length cDNAs of *PbrPPA5* and *PbrbZIP77* were amplified using PCR and cloned into an overexpression vector driven by the 35S promoter to generate *35Spro:PbrPPA5* and

35Spro:*PbrbZIP77* (Xie et al., 2014). Point mutations (*PbrPPA5*<sup>K42R</sup>, *PbrPPA5*<sup>K42Q</sup>, *PbrPPA5*<sup>D136N</sup> and *PbrPPA5*<sup>P137A</sup>) were introduced using a Fast Mutagenesis System (Transgen, China). The 1.3-kbp promoter sequence of *PbrPME44* was amplified by PCR, and the PCR-amplified fragments were then cloned into a pGreenII 0800-LUC vector to generate *PbrPME44pro:LUC*. Primers are listed in Supplemental Data Set S3. The Renilla luciferase gene (*REN*) driven by the 35S promoter was used in the pGreenII 0800-LUC as the internal control. The dual-luciferase reporter assays in *Nicotiana benthamiana* leaves were performed as described previously (Hellens et al., 2005). Relative luciferase activities were quantified using the Dual-Luciferase Reporter Assay System (Promega, USA) with CYTATION3 microplate readers (BioTek, USA). At least three independent experiments were performed.

### Sequence analysis

The sequence of *AtbZIP34* was retrieved from TAIR 10 (<http://www.arabidopsis.org/>). Sequences of the Prp26.1a/b proteins from poppy were downloaded from NCBI (<https://www.ncbi.nlm.nih.gov/>). Multiple sequence alignments were performed using DNAMAN (<https://www.lynnon.com/qa.html>).

### Y2H assays

A cDNA library for Y2H assay was constructed by Clontech (Takara, Japan) from the total RNA of Dangshansuli pollen. Full-length cDNAs of *PbrbZIP77* and *PbrPPA5* were cloned into the pGBKT7 vector (Clontech, USA) to be used as bait for screening the cDNA library using the Matchmaker Gold System (Clontech, USA). The screening was performed on SD/-Trp-Leu-His medium according to the manufacturer's instructions.

For the protein-protein interaction assay, full-length cDNAs of *PbrbZIP77*, *PbrPPA5*, *PbrS7-RNase* and *PbrS34-RNase* were cloned into pGADT7 AD (Clontech, USA). *PbrPPA1*, *PbrPPA2*, *PbrPPA5*, *PbrPPA9*, *PbrPPA10*, and *PbrGNAT1* were cloned into pGBKT7 vectors individually. Point mutations (*PbrPPA5*<sup>D136N</sup> and *PbrPPA5*<sup>P137A</sup>) were introduced into *PbrPPA5* using a Fast Mutagenesis System kit (Transgen, China). After mutation, *PbrPPA5*<sup>D136N</sup> and *PbrPPA5*<sup>P137A</sup> were inserted into pGBKT7 vectors individually. The coding sequences of different domains in *PbrPPA5* (1–31, 32–54, 55–86, 87–213, 214–234, and 235–248 aa) were cloned into pGBKT7 vectors individually. All interactions were detected by co-transforming plasmids into the yeast strain AH109.

---

The interactions were assessed on SD/-Trp-Leu-Ade-His medium. pGBKT7-P53 and pGADT7-T were used as a positive control, and pGBKT-Lam and pGADT7-T were a negative control. All the primers are listed in Supplemental Data Set S3.

### **LCI assay**

*PbrPPA5* and *PbrbZIP77* were amplified using PCR and cloned into the pCAMBIA1300-CLuc and pCAMBIA1300-NLuc vectors to generate *PbrPPA5-CLuc* and *PbrbZIP77-NLuc*, respectively (Zhou et al., 2018). These two constructs were transformed into *N. benthamiana* leaves using *Agrobacterium tumefaciens*-mediated transformation (Sparkes et al., 2006) and the luciferase complementation assay for *PbrPPA5* and *PbrbZIP77* interaction was performed as described previously (Zhou et al., 2018). Luminescence in *N. benthamiana* leaves was photographed by a CCD imaging system (PIXIS 1024B, Princeton Instruments, USA).

### **BiFC assay**

*PbrPPA5*, *PbrbZIP77*, and *PbrGNAT1* were cloned into the pSPYNE-35S and pSPYCE-35S vectors to generate *PbrPPA5-YNE*, *PbrbZIP77-YCE*, and *PbrGNAT1-YCE*, respectively (Walter et al., 2004). These constructs were transformed into *N. benthamiana* leaf cells using *Agrobacterium*-mediated transformation (Sparkes et al., 2006). After 3 days of cultivation, tobacco leaves were harvested, stained with DAPI (Thermo Fisher Scientific, USA) as a nucleus marker, and used for imaging. Fluorescence signals were imaged using a LSM800 confocal microscope (Carl Zeiss, Germany). The excitation wavelength and transmission range for emission were 488 nm/500-550 nm for the GFP channel, and the detector gain was 700 V.

### **MST assay**

The MST assay was performed using the Monolith NT.115 instrument (Nano Temper Technologies, Germany) according to the manufacturer's instructions. For protein labeling, the Monolith His-Tag Labeling Kit RED-tris-NTA (Nano Temper Technologies, Germany) was used following the manufacturer's procedure. The purified His-tagged protein, rPbrbZIP77, was concentrated in the labelling buffer (PBS plus 0.5% Tween) by centrifugal ultrafiltration (6,000 *g*, 5 min) to a final concentration of 50 nM. For the binding assay, serial 2-fold dilutions of 16 concentrations (initiated

---

from 1000 nM) of the protein ligands (rPbrPPA5, rPbrPPA5<sup>K42Q</sup>, or rPbrPPA5<sup>K42R</sup>) were tested. The labelled rPbrbZIP77 and diluted ligands were mixed into the capillary and analyzed using the Monolith NT.115 instrument. Proteins purified from the empty pCold-TF vector were used as negative controls. MST curves for each capillary were recorded and the  $K_d$  of each reaction was calculated using the MO Affinity Analysis software v1.6 (Nano Temper Technologies, Germany). Three biological replicates were employed for each combination.

### Measurement of PME activity

Pollen tube samples were collected by centrifugation (13,500 g, 1 min) and then ground in liquid nitrogen. Crude proteins were extracted using a Plant Protein Extraction Kit (Solarbio, China). Protein concentrations were measured using the Modified Bradford reagent (Sangon, China) with bovine serum albumin as a standard. PME activity was measured as described previously (Downie et al., 1998). In brief, gels were prepared using 0.1% of pectin from citrus (P0024, TCI, Japan), 2% (w/v) agarose (low melting point gel), 0.1 M citric acid, and 0.2 mM Na<sub>2</sub>HPO<sub>4</sub> (pH 7.0). Wells (4 mm diameter) were punched by injector, and 5 µg of each crude proteins were loaded into each well. The plates were then incubated at 30°C for 16 h, gels were stained with 0.05% (w/v) ruthenium red for 45 min, then washed thoroughly with distilled water. The diameter of the red-stained areas determined by caliper was indicative of the hydrolysis of esterified pectin in the gels. At least three biological replicates were employed for each treatment.

### Pyrophosphatase activity assay

To determine sPPase activity, 500 ng rPbrPPA5, rPbrPPA5<sup>K42Q</sup>, rPbrPPA5<sup>K42R</sup>, rPbrPPA5<sup>D136N</sup>, or rPbrPPA5<sup>P137A</sup> were added into 200 µL reaction buffer (1 mM PPi, 5 mM MgCl<sub>2</sub>, 100 mM Tris-HCl pH 7.0) and incubated for 15 min at 37°C. For pollen samples, 200 mg pollen was collected and extracted using a Plant Protein Extraction Kit (Solarbio, China). The reaction was stopped by adding 5% trichloroacetic acid (TCA) and then assayed as described previously (Visser et al., 1998; de Graaf et al., 2006).

### as-ODN treatment

An as-ODN experiment was performed as previously described (Moutinho et al., 2001). Both

---

phosphorothioated as-ODN and phosphorothioated s-ODN were designed using the RNA fold web server (<http://rna.tbi.univie.ac.at/cgi-bin/RNAfold.cgi>). For the as-ODN and s-ODN treatments, pollen was pre-cultured in liquid germination medium for 1 h, then 6  $\mu$ L as-ODNs (30  $\mu$ M) or s-ODNs was mixed with 12.5  $\mu$ L germination media and 1.5  $\mu$ L cytofectin (Lipofectamine 2000, Thermo Fisher Scientific, USA) for 15 min before being added to 180  $\mu$ L cultivated pollen. Pollen treated with cytofectin and germination medium only was used as a control. The sequences of the phosphorothioated ODNs are listed in Supplemental Data Set S3.

### **Nuclear fractionation assay of pollen tubes and tobacco leaves**

Nuclei were extracted by nuclear fractionation, as described previously (Gao et al., 2015). Pollen tubes were overlaid with nuclei isolation buffer (0.3 M sucrose, 10 mM NaCl, 10 mM 2-(N-morpholine)-ethanesulfonic acid, 5 mM ethylenediamine-tetraacetic acid, 0.2 mM spermine, 0.5 mM spermidine, 0.2 mM phenylmethylsulphonyl fluoride, 5 mM dithiothreitol, and 0.2% (v/v) Triton-X-100, adjusted to pH 7.4 with 2 M NaOH), separated by filtration in a cell strainer I (40  $\mu$ m pore size) with homogenizing by a glass pestle, and collected in an open Petri dish under a cell strainer II (25  $\mu$ m pore size). After centrifugation at 200 g at 4°C for 3 min, the supernatant was separated and then placed onto a 28% (v/v) Percoll™ solution (diluted in nuclei isolation buffer) (GE Healthcare, USA). After centrifugation at 3,000 g for 20 min, the purified nuclei were located at the bottom of the Percoll layer and the upper phase was the cytoplasmic fraction. All the above steps were performed at 4°C. Protein extracts of tobacco leaf nuclei were obtained using a Nuclear Protein Extraction Kit (Solarbio, China). Crude proteins were extracted using a Plant Protein Extraction Kit (Solarbio, China). All the above steps were performed at 4°C.

### **Immunoblotting**

Pollen tubes were collected after 1.5-h mock, CS, and IS treatments. Nuclear/cytosolic protein extracts of pear pollen tubes were prepared as described above. Protein extracts were separated using 12% sodium dodecyl sulfate-polyacrylamide gel electrophoresis (SDS-PAGE) and transferred onto an Immobilon-P PVDF membrane (MilliporeSigma, USA). After blocking with 5% solution of nonfat milk powder in Tris buffered saline containing 0.1% Tween (pH 8.0), the membrane filter was incubated with the anti-PbrPPA5 rabbit polyclonal primary antibody

---

(LPTLQAFEVQKLMASEDQSEEAK; 1:1,000 dilution) overnight, followed by incubation with an HRP-conjugated goat anti-rabbit IgG antibody (1:5,000 dilution) (Sangon, China) for 2 h at room temperature. The chemiluminescence reagent ECL substrate (Thermo Fisher Scientific, USA) was used for antigen detection, and chemiluminescence was detected using a ChemiDoc MP Imaging System (Bio-Rad, USA). Anti-HA tag mouse monoclonal antibody (1:2,000 dilution; Beyotime, China) was added to detect the presence of PbrGNAT1-HA, and an anti-GFP rabbit polyclonal antibody (1:2,000 dilution; Sangon, China) was added to detect the presence of PbrPPA5-GFP. Anti-histone H3 mouse monoclonal antibody (1:2,000 dilution; Beyotime, China), Anti-histone H3.3 rabbit monoclonal antibody (1:1,000 dilution; Beyotime, China) and anti-GAPDH rabbit polyclonal antibody (1:2,000 dilution; Sangon, China) were used as the loading controls for nuclear and cytoplasmic proteins, respectively.

### Subcellular localization

Full-length cDNA of *PbrPPA5* lacking the stop codon was amplified using PCR then cloned into *pCAMBIA1300-35S:CDS-GFP* (Xie et al., 2014). Point mutations (PbrPPA5<sup>K9R</sup>, PbrPPA5<sup>K9Q</sup>, PbrPPA5<sup>K42R</sup>, PbrPPA5<sup>K42Q</sup>, PbrPPA5<sup>K98R</sup>, and PbrPPA5<sup>K98Q</sup>) were introduced using a Fast Mutagenesis System (Transgen, China). Full-length cDNA of *PbrGNAT1* lacking the stop codon was cloned into an overexpression vector (*pCAMBIA1300-35S:CDS-HA*) driven by the 35S promoter to generate the 35Spro:PbrGNAT1-HA vector (Xie et al., 2014). Primers are listed in Supplemental Data Set S3. Constructs were transformed into *Agrobacterium* strain GV3101 and the transformed cells were infiltrated into *N. benthamiana* leaf epidermal cells using *Agrobacterium*-mediated transformation (Sparkes et al., 2006). The blue-fluorescent dye DAPI (Sigma-Aldrich, USA) was used as a nuclear marker. All fluorescence imaging was performed using a LSM800 confocal microscope with airyscan (Carl Zeiss, Germany) and quantified using ZEN imaging software (Carl Zeiss, Germany). The excitation wavelength and transmission range for emission were 488 nm/500-550 nm for the GFP channel and 405 nm/400-490 nm for the DAPI channel. The detector gain was 700 V.

### Detection of PbrPPA5 modifications during SI using liquid chromatography–tandem mass spectrometry

---

Pollen was grown in liquid germination medium for 1.5 h at 25°C and was then subjected to IS and CS treatments for 1.0 h, 1.5 h, and 2.0 h. Pollen samples were collected by centrifugation at 6,000 g for 1 min. After samples were ground in liquid nitrogen, crude proteins were extracted using the Plant Protein Extraction Kit (Solarbio, China). Protein concentrations were measured using a NanoDrop 2000 (Thermo Fisher Scientific, USA). To detect the modification of PbrPPA5 resulting from CS and IS treatments, crude proteins were separated using 12% SDS-PAGE and the bands corresponding to the molecular weight of PbrPPA5 were cut from the gel and sent for mass-spectrometric analysis. Mass spectrometry was performed by Shanghai Applied Protein Technology (Shanghai, China) using Q Exactive and Easy-nLC 1000 (Thermo Fisher Scientific, USA). The resulting data were analyzed using Proteome Discoverer1.4 (Thermo Fisher Scientific, USA) and MASCOT (<http://www.matrixscience.com>).

### Particle bombardment

Full-length cDNAs of *PbrPPA5*, *PbrPPA5*<sup>K42Q</sup> and *PbrPPA5*<sup>K42R</sup> were amplified using PCR and individually cloned into an overexpression vector driven by the NTP303 promoter (X69440.1) to generate *NTP303pro:PbrPPA5*, *NTP303pro:PbrPPA5*<sup>K42Q</sup> and *NTP303pro:PbrPPA5*<sup>K42R</sup>. A sequence encoding AtH2B-mCherry was cloned to the same vector and used as a nuclei marker (Motomura et al., 2021). Recombinant plasmids were isolated using a FastPure EndoFree Plasmid Maxi Kit (Vazyme, China) and transiently expressed in pear pollen using a PDS-1000/He particle bombardment device (Bio-Rad, USA) according to a previously described protocol with some modification (Qian et al. 2020). A mixture of 8.5 µL gold particles (Bio-Rad, USA) and 10 µL of 0.15 M spermidine, 2.5 µL of 2 µg/µL recombinant plasmid and 29 µL of 2 M CaCl<sub>2</sub> was used, with constant vortexing for 3 min. The gold microcarriers were centrifuged at 9,500 g for 5 s and the supernatant was removed. Then, the gold particles were washed with 200 µL of absolute ethanol and centrifuged at 9,500 g for 5 s. Finally, the gold particles were resuspended in 20 µL of absolute ethanol for transformation. The settings of the PSD-1000/He particle delivery system were as follows: 1,350 psi, 20-mm Hg vacuum, 1-cm gap distance between the rupture disk and macrocarrier, and 9-cm particle flight distance between macrocarrier and pollen samples. The pollen samples were placed on solid germination medium (containing 1.5% agarose) prior to transformation. For DAPI staining, pollen tubes were fixed in 4% paraformaldehyde for 30 min and stained with DAPI.

---

Fluorescence images were performed using a LSM800 confocal microscope (Carl Zeiss, Germany). The excitation wavelength and transmission range for emission were 488 nm/500-550 nm for GFP, 405 nm/400-490 nm for DAPI, and 561 nm/570-700 nm for mCherry. The detector gain was 700 V.

### **Immunoprecipitation (IP) and acetylation assays**

For IP assays, *Agrobacterium* strain GV3101 containing PbrPPA5-GFP, PbrPPA5<sup>K42R</sup>-GFP, or PbrGNAT1-HA was used as mentioned (Sparkes et al., 2006). Cells transformed with PbrPPA5-GFP, or PbrPPA5<sup>K42R</sup>-GFP were mixed with the strain containing PbrGNAT1-HA at OD<sub>600</sub> = 0.6-0.8 and infiltrated into *N. benthamiana* leaves using *Agrobacterium*-mediated transformation (Sparkes et al., 2006). After 3 d, the total proteins or nuclear proteins were extracted and incubated with GFP nanoantibody coupled magnetic beads (Nucleotech Scientific, China) at 4 °C for 30 min. After incubation, the antigen-antibody complex was collected using a magnetic separator (Thermo Fisher Scientific, USA; 12321D) and washed 3 times with wash buffer (50 mM Tris-HCl, pH 7.5, 150 mM NaCl, 0.5 mM EDTA pH 8.0, 0.5% IGEPAL CA-630), then boiled with 5× SDS sample buffer for immunoblotting. The immunoprecipitates were separated by 12% SDS-PAGE and detected with anti-acetylated lysine mouse antibody (1:1000 dilution; PTM Biolabs, China) which recognized any proteins acetylated on lysine residues. Immunoblotting with an anti-HA tag mouse monoclonal antibody or anti-GFP rabbit polyclonal antibody was used as the loading control.

### **Statistical analysis**

All experimental data were analyzed by SPSS version 22. Multiple samples were analyzed using one-way ANOVA followed by Tukey's difference test. The summary of statistical analyses is listed in Supplemental Data Set S4.

### **Accession numbers**

Sequence data from this article can be found in the GenBank/EMBL libraries under the following accession numbers: *PbrPPA5* (MN610578), *PbrGNAT1* (XP\_009352002.1), *PbrPME44* (XP\_009352341.1), *PbrbZIP77* (XP\_018503142.1), *PbrTUB-2* (XP\_009374320.1) and *NTP303* (X69440.1). The data that support the findings of this study are available from the corresponding authors upon reasonable request. The sequences of the genes and proteins mentioned in this article

---

are available for download at the Pear Genome Project (<http://peargenome.njau.edu.cn>). The raw transcriptome data reported in this paper have been deposited in the Genome Sequence Archive (Chen et al., 2021) at the National Genomics Data Center (CNCB-NGDC Members and Partners, 2020), China National Center for Bioinformation/Beijing Institute of Genomics, Chinese Academy of Sciences (PRJCA007552) and are publicly accessible at <https://ngdc.cncb.ac.cn/gsa>.

ACCEPTED MANUSCRIPT

---

## Funding information

This work was supported by the National Key Research and Development Program of China (2022YFD1200503, 2022YFF1003100-02, 2020YFE0202900), the National Natural Science Foundation of China (32172543, 32102358, 31830081), the Jiangsu Agricultural Science and Technology Innovation Fund (CX(22)3044), the Fundamental Research Funds for the Central Universities (JCQY202103), the Priority Academic Program Development of Jiangsu Higher Education Institutions, the Natural Science Foundation of Jiangsu Province (BK20210394), Hainan Yazhou Bay Seed Lab Project (B22E11002) and the Earmarked Fund for China Agriculture Research System (CARS-28).

## Acknowledgments

We would like to thank the Bioinformatics Center of Nanjing Agricultural University for support with bioinformatic analysis. We would also like to thank Plant Editors for English language editing.

## Author contributions

J.Y.W., S.L.Z, C.T., and P.W. conceived and designed the experiments; C.T., and P.W., X.X.Z., H.Z., X.Q.L., and H.R.G. performed the experiments. J.Y.W., C.T., and P.W. wrote the manuscript; B.H.J.d.G, T.T.G., S.L, K.J.Q., Z.H.X., C.G., and S.L.Z critically read and commented on the manuscript. All authors have read and approved of the manuscript.

## Conflict of interest statement.

The authors declare no conflict of interest.

## References

- Anderson, M.A., Cornish, E.C., Mau, S.-L., Williams, E.G., Hoggart, R., Atkinson, A., Bonig, I., Grego, B., Simpson, R., Roche, P.J., Haley J.D., Penschow J.D., Niall H.D., Tregear G.W., Coghlan J.P., Crawford R.J., and Clarke A.E. (1986).** Cloning of cDNA for a stylar glycoprotein associated with expression of self-incompatibility in *Nicotiana alata*. *Nature* **321**: 38-44.
- Baeza, J., Smallegan, M.J., and Denu, J.M. (2016).** Mechanisms and dynamics of protein

---

acetylation in mitochondria. Trends Biochem. Sci. **41**: 231-244.

- Bosch, M., and Hepler, P.K.** (2005). Pectin methylesterases and pectin dynamics in pollen tubes. Plant Cell **17**: 3219-3226.
- Bosch, M., and Franklin-Tong, V.E.** (2007). Temporal and spatial activation of caspase-like enzymes induced by self-incompatibility in *Papaver* pollen. Proc. Natl. Acad. Sci. USA **104**: 18327-18332.
- Bosch, M., Cheung, A.Y., and Hepler, P.K.** (2005). Pectin methylesterase, a regulator of pollen tube growth. Plant Physiol. **138**: 1334-1346.
- Brugière, N., Rothstein, S.J., and Cui, Y.** (2000). Molecular mechanisms of self-recognition in *Brassica* self-incompatibility. Trends Plant Sci. **5**: 432-438.
- Chebli, Y., Kaneda, M., Zerzour, R., and Geitmann, A.** (2012). The cell wall of the Arabidopsis pollen tube—spatial distribution, recycling, and network formation of polysaccharides. Plant Physiol. **160**: 1940-1955.
- Chen, C., Chen, H., Zhang, Y., Thomas, H.R., Frank M.H., He Y., and Xia, R.** (2020). TBtools: an integrative toolkit developed for interactive analyses of big biological data. Mol. Plant **13**: 1194-1202.
- Chen, J., Wang, P., de Graaf, B.H.J., Zhang, H., Jiao, H., Tang, C., Zhang, S., and Wu, J.** (2018). Phosphatidic acid counteracts S-RNase signaling in pollen by stabilizing the actin cytoskeleton. Plant Cell **30**: 1023-1039.
- Chen, T., Chen, X., Zhang, S., Zhu, J., Tang, B., Wang, A., Dong, L., Zhang, Z., Yu, C., Sun, Y., Chi, L., Chen, H., Zhai, S., Sun, Y., Lan, L., Zhang, X., Xiao, J., Bao, Y., Wang, Y., Zhang, Z., and Zhao, W.** (2021). The genome sequence archive family: toward explosive data growth and diverse data types. Genom. Proteom. Bioinf. **19**: 578-583.
- Cheung, A.Y.** (2022). Self-incompatibility in *Papaver rhoeas*: a role for ATP. New Phytol. **236**: 1625-1628.
- CNCB-NGDC Members, and Partners.** (2020). Database resources of the National Genomics Data Center, China National Center for Bioinformatics in 2021. Nucleic Acids Res. **49**: D18-D28.
- de Graaf, B.H.J., Rudd, J.J., Wheeler, M.J., Perry, R.M., Bell, E.M., Osman, K., Franklin, F.C.H., and Franklin-Tong, V.E.** (2006). Self-incompatibility in *Papaver* targets soluble inorganic pyrophosphatases in pollen. Nature **444**: 490-493.

- 
- de Nettancourt, D.** (2001). Incompatibility and incongruity in wild and cultivated plants. Springer, Berlin, Heidelberg.
- Downie, B., Dirk, L.M., Hadfield, K.A., Wilkins, T.A., Bennett, A.B., and Bradford, K.J.** (1998). A gel diffusion assay for quantification of pectin methylesterase activity. *Anal. Biochem.* **264**: 149-157.
- Drazic, A., Myklebust, L.M., Ree, R., and Arnesen, T.** (2016). The world of protein acetylation. *Biochim. Biophys. Acta.* **1864**: 1372-1401.
- Duan, Q., Liu, M.J., Kita, D., Jordan, S.S., Yeh F.J., Yvon R., Carpenter H., Federico A.N., Garcia-Valencia L.E., Eyles S.J., Wang C.S., Wu H.M., and Cheung, A.Y.** (2020). FERONIA controls pectin- and nitric oxide-mediated male–female interaction. *Nature* **579**: 561-566.
- Eaves, D.J., Haque, T., Tudor, R.L., Barron, Y., Zampronio, C.G., Cotton, N.P.J., De Graaf, B.H.J., White, S.A., Cooper, H.J., Franklin F.C.H., Harper J.F., and Franklin-Tong, V.E.** (2017). Identification of phosphorylation sites altering pollen soluble inorganic pyrophosphatase activity. *Plant Physiol.* **173**: 1606-1616.
- Franklin-Tong, N.V., and Franklin, F.C.H.** (2003). Gametophytic self-incompatibility inhibits pollen tube growth using different mechanisms. *Trends Plant Sci.* **8**: 598-605.
- Fujii, S., Kubo, K., and Takayama, S.** (2016). Non-self- and self-recognition models in plant self-incompatibility. *Nat. Plants* **2**: 16130.
- Gao, Y., Wang, C., Wu, J., Wu, J., Zhou, H., and Zhang, S.** (2015). A method to isolate male gametic nuclei from pear pollen tubes. *J. Hortic. Sci. Biotech.* **88**: 313-319.
- Gdula, D.A., Sandaltzopoulos, R., Tsukiyama, T., Ossipow, V., and Wu, C.** (1998). Inorganic pyrophosphatase is a component of the *Drosophila* nucleosome remodeling factor complex. *Genes Dev.* **12**: 3206-3216.
- Geitmann, A., and Steer, M.** (2006). The architecture and properties of the pollen tube cell wall, in *The Pollen Tube: a cellular and molecular perspective* (Malhó R. ed), Springer Berlin Heidelberg, Berlin, Heidelberg. pp: 177-200.
- Gibalová, A., Reňák, D., Matczuk, K., Dupl'Áková, N., Cháb, D., Twell, D., and Honys, D.** (2009). *AtbZIP34* is required for Arabidopsis pollen wall patterning and the control of several metabolic pathways in developing pollen. *Plant Mol. Biol.* **70**: 581-601.

- 
- Goldraj, A., Kondo, K., Lee, C.B., Hancock, C.N., Sivaguru, M., Vazquez-Santana, S., Kim, S., Phillips, T.E., Cruz-garcia, F., and McClure, B.A.** (2006). Compartmentalization of S-RNase and HT-B degradation in self-incompatible *Nicotiana*. *Nature* **439**: 805-810.
- Gray, J.E., McClure, B.A., Bonig, I., Anderson, M.A., and Clarke, A.E.** (1991). Action of the style product of the self-incompatibility gene of *Nicotiana alata* (S-RNase) on in vitro-grown pollen tubes. *Plant Cell* **3**: 271-283.
- Grzechowiak, M., Ruszkowski, M., Sliwiak, J., Szpotkowski, K., Sikorski, M., and Jaskolski, M.** (2019). Crystal structures of plant inorganic pyrophosphatase, an enzyme with a moonlighting autoproteolytic activity. *Biochem. J.* **476**: 2297-2319.
- Haas, K.T., Wightman, R., Meyerowitz, E.M., and Peaucelle, A.** (2020). Pectin homogalacturonan nanofilament expansion drives morphogenesis in plant epidermal cells. *Science* **367**: 1003-1007.
- Hellens, R.P., Allan, A.C., Friel, E.N., Bolitho, K., Grafton, K., Templeton, M.D., Karunairetnam, S., Gleave, A.P., and Laing, W.A.** (2005). Transient expression vectors for functional genomics, quantification of promoter activity and RNA silencing in plants. *Plant Methods* **1**: 13.
- Hiratsuka, S., and Tezuka, T.** (1980). Changes in proteins in pistils after self- and cross-pollination in Japanese pear. *Engei Gakkai Zasshi* **49**: 57-64.
- Jia, H., He, F., Xiong, C., Zhu, F., and Okamoto G.** (2008). Influences of cross pollination on pollen tube growth and fruit set in Zuili plums (*Prunus salicina*). *J. Integr. Plant Biol.* **50**: 203-209.
- Jiang, L., Yang, S., Xie, L.F., Pua, C.S., Zhang, X.Q., Yang, W.C., Sundaresan, V., and Ye, D.** (2005). *VANGUARD1* encodes a pectin methylesterase that enhances pollen tube growth in the Arabidopsis style and transmitting tract. *Plant Cell* **17**: 584-596.
- Kao, T.H., and McCubbin, A.G.** (1996). How flowering plants discriminate between self and non-self pollen to prevent inbreeding. *Proc. Natl. Acad. Sci. USA* **93**: 12059-12065.
- Kim, S.C., Sprung, R., Chen, Y., Xu, Y., Ball, H., Pei, J., Cheng, T., Kho, Y., Xiao, H., Xiao, L., Grishin, N.V., White, M., Yang, X.J., and Zhao, Y.** (2006). Substrate and functional diversity of lysine acetylation revealed by a proteomics survey. *Mol. Cell* **23**: 607-618.
- Kim, Y.J., Jeong, H.Y., Kang, S.Y., Silva, J., Kim, E.J., Park, S.K., Jung, K.H., and Lee, C.** (2020). Physiological importance of pectin modifying genes during rice pollen development. *Int. J.*

- Li, W., Meng, D., Gu, Z., Yang, Q., Yuan, H., Li, Y., Chen, Q., Yu, J., Liu, C., and Li, T.** (2018). Apple S-RNase triggers inhibition of tRNA aminoacylation by interacting with a soluble inorganic pyrophosphatase in growing self-pollen tubes *in vitro*. *New Phytol.* **218**: 579-593.
- Liang, M., Cao, Z., Zhu, A., Liu, Y., Tao, M., Yang, H., Xu, Q., Jr., Wang, S., Liu, J., Li, Y., Chen, C., Xie, Z., Deng, C., Ye, J., Guo, W., Xu, Q., Xia, R., Larkin, R.M., Deng, X., Bosch, M., Franklin-Tong, V.E., and Chai, L.** (2020). Evolution of self-compatibility by a mutant *S<sub>m</sub>-RNase* in citrus. *Nat. Plants* **6**: 131-142.
- Lin, Z., Xie, F., Triviño, M., Zhao, T., Coppens, F., Sterck, L., Bosch, M., Franklin-Tong, V.E., and Nowack, M.K.** (2022). Self-incompatibility requires GPI anchor remodeling by the poppy PGAP1 ortholog HLD1. *Curr. Biol.* **32**: 1909-1923.
- Liu, Z., Xu, G., and Zhang, S.** (2007). *Pyrus pyrifolia* stylar S-RNase induces alterations in the actin cytoskeleton in self-pollen and tubes *in vitro*. *Protoplasma* **232**: 61-67.
- Livak, K.J., and Schmittgen, T.D.** (2001). Analysis of relative gene expression data using real-time quantitative PCR and the 2<sup>-ΔΔCT</sup> Method. *Methods* **25**: 402-408.
- Love, M.I., Huber, W., and Anders, S.** (2014). Moderated estimation of fold change and dispersion for RNA-seq data with DESeq2. *Genome Biol.* **15**: 550.
- Lu, Y., Hokin, S.A., Kermicle, J.L., Hartwig, T., and Evans, M.M.S.** (2019). A pistil-expressed pectin methylesterase confers cross-incompatibility between strains of *Zea mays*. *Nat. Commun.* **10**: 2304.
- Luu, D., Qin, X., Morse, D., and Cappadocia, M.** (2000). S-RNase uptake by compatible pollen tubes in gametophytic self-incompatibility. *Nature* **407**: 649-651.
- Ma, M., Chen, Q., Dong, H., Zhang, S., and Huang, X.** (2021) Genome-wide identification and expression analysis of the bZIP transcription factors, and functional analysis in response to drought and cold stresses in pear (*Pyrus breschneideri*). *BMC Plant Biol.* **21**: 583.
- McClure, B.A., Gray, J.E., Anderson, M.A., and Clarke, A.E.** (1990). Self-incompatibility in *Nicotiana alata* involves degradation of pollen rRNA. *Nature* **347**: 757-760.
- McClure, B.A., Haring, V., Ebert, P.R., Anderson, M.A., Simpson, R.J., Sakiyama, F., and Clarke, A.E.** (1989). Style self-incompatibility gene products of *Nicotiana alata* are ribonucleases. *Nature* **342**: 955-957.

- 
- Motomura, K., Takeuchi, H., Notaguchi, M., Tsuchi, H., Takeda, A., Kinoshita, T., Higashiyama, T., and Maruyama, D.** (2021). Persistent directional growth capability in *Arabidopsis thaliana* pollen tubes after nuclear elimination from the apex. *Nat. Commun.* **12**: 2331.
- Moutinho, A., Camacho, L., Haley, A., Pais, M.S., Trewavas, A., and Malhó, R.** (2001). Antisense perturbation of protein function in living pollen tubes. *Sex. Plant Reprod.* **14**: 101-104.
- Narita, T., Weinert, B.T., and Choudhary, C.** (2019). Functions and mechanisms of non-histone protein acetylation. *Nat. Rev. Mol. Cell Biol.* **20**: 156-174.
- Newbigin, E., Anderson, M.A., and Clarke, A.E.** (1993). Gametophytic self-incompatibility systems. *Plant Cell* **5**: 1315-1324.
- Parre, E., and Geitmann, A.** (2005). Pectin and the role of the physical properties of the cell wall in pollen tube growth of *Solanum chacoense*. *Planta* **220**: 582-592.
- Parrotta, L., Faleri, C., Guerriero, G., and Cai, G.** (2019). Cold stress affects cell wall deposition and growth pattern in tobacco pollen tubes. *Plant Sci.* **283**: 329-342.
- Qian, M., Xu, L., Tang, C., Zhang, H., Gao, H., Cao, P., Yin, H., Wu, L., Wu, J., Gu, C., and Zhang, S.** (2020). *PbrPOE21* inhibits pear pollen tube growth in vitro by altering apical reactive oxygen species content. *Planta*. **252**: 43.
- Rêgo, M.M., Rêgo, E.R., Bruckner, C.H., Da Silva, E.A.M., Finger, F.L., and Pereira, K.J.C.** (2000). Pollen tube behavior in yellow passion fruit following compatible and incompatible crosses. *Theor. Appl. Genet.* **101**: 685-689.
- Sassa, H., Hirano, H., and Ikehashi H.** (1992). Self-incompatibility-related RNases in styles of Japanese pear (*Pyrus serotina* Rehd.). *Plant Cell Physiol.* **6**: 811-814.
- Segami, S., Tomoyama, T., Sakamoto, S., Gunji, S., Fukuda, M., Kinoshita, S., Mitsuda, N., Ferjani, A., and Maeshima, M.** (2018). Vacuolar H<sup>+</sup>-pyrophosphatase and cytosolic soluble pyrophosphatases cooperatively regulate pyrophosphate levels in *Arabidopsis thaliana*. *Plant Cell* **30**: 1040-1061.
- Silva-Sanzana, C., Celiz-Balboa, J., Garzo, E., Marcus, S.E., Parra-Rojas, J.P., Rojas, B., Olmedo, P., Rubilar, M.A., Rios, I., Chorbadian, R.A., Fereres, A., Knox, P., Saez-Aguayo, S., and Blanco-Herrera, F.** (2019). Pectin methylesterases modulate plant gomogalacturonan status in defenses against the Aphid *Myzus persicae*. *Plant Cell* **31**: 1913-1929.

- 
- Silva, N.F., and Goring, D.R.** (2001). Mechanisms of self-incompatibility in flowering plants. *Cell. Mol. Life Sci.* **58**: 1988-2007.
- Sparkes, I.A., Runions, J., Kearns, A., and Hawes, C.** (2006). Rapid, transient expression of fluorescent fusion proteins in tobacco plants and generation of stably transformed plants. *Nat. Protoc.* **1**: 2019-2025.
- Sun, L., Cao, S., Zheng, N., and Kao, T.H.** (2022). Analyses of Cullin1 homologs reveal functional redundancy in S-RNase-based self-incompatibility and evolutionary relationships in eudicots. *Plant Cell.* **35**: 673-699.
- Tang, C., Qiao, X., Zhu, X., Khan, W., Wu, J., and Zhang, S.** (2020a). Expression and evolutionary analysis of soluble inorganic pyrophosphatase gene family in pear and four other Rosaceae species. *Plant Syst. Evol.* **306**: 46.
- Tang, C., Zhu, X., Qiao, X., Gao, H., Li, Q., Wang, P., Wu, J., and Zhang, S.** (2020b). Characterization of the pectin methyl-esterase gene family and its function in controlling pollen tube growth in pear (*Pyrus bretschneideri*). *Genomics* **112**: 2467-2477.
- Thomas, S.G., and Franklin-Tong, V.E.** (2004). Self-incompatibility triggers programmed cell death in *Papaver* pollen. *Nature* **429**: 305-309.
- Tian, G.W., Chen, M.H., Zaltsman, A., and Citovsky, V.** (2006). Pollen-specific pectin methylesterase involved in pollen tube growth. *Dev. Biol.* **294**: 83-91.
- Visser, K., Heimovaara-Dijkstra, S., Kijne, J.W., and Wang, M.** (1998). Molecular cloning and characterization of an inorganic pyrophosphatase from barley. *Plant Mol. Biol.* **37**: 131-140.
- Walter, M., Chaban, C., Schütze, K., Batistic, O., Weckermann, K., Näke, C., Blazevic, D., Grefen, C., Schumacher, K., Oecking, C., Harter K., and Kudla, J.** (2004). Visualization of protein interactions in living plant cells using bimolecular fluorescence complementation. *Plant J.* **40**: 428-438.
- Wang, C., Xu, G., Jiang, X., Gong, C., Wu, J., Wu, H., and Zhang, S.** (2009). S-RNase triggers mitochondrial alteration and DNA degradation in the incompatible pollen tube of *Pyrus pyrifolia* *in vitro*. *Plant J.* **57**: 220-229.
- Wang, C., Wu, J., Xu, G., Gao, Y., Chen, G., Wu, J., Wu, H., and Zhang, S.** (2011). S-RNase disrupts tip-localized reactive oxygen species and induces nuclear DNA degradation in incompatible pollen tubes of *Pyrus pyrifolia*. *J. Cell Sci.* **123**: 4301-4309.

- Wang, D., Samsulrizal, N.H., Yan, C., Allcock, N.S., Craigon, J., Blanco-Ulate, B., Ortega-Salazar, I., Marcus, S.E., Bagheri, H.M., Perez Fons, L., Fraser, P.D., Foster, T., Fray, R., Knox, J.P., and Seymour, G.B. (2019). Characterization of CRISPR mutants targeting genes modulating pectin degradation in ripening tomato. *Plant Physiol.* **179**: 544-557.
- Wang, H., Holloway, M.P., Ma, L., Cooper, Z.A., Riolo, M., Samkari, A., Elenitoba-Johnson, K.S.J., Chin, Y.E., and Altura, R.A. (2010). Acetylation directs survivin nuclear localization to repress STAT3 oncogenic activity. *J. Biol. Chem.* **285**: 36129-36137.
- Wang, L., Lin, Z., Carli, J., Gladala-Kostarz, A., Davies, J.M., Franklin-Tong, V.E., and Bosch, M. (2022). Depletion plays a pivotal role in self-incompatibility, revealing a link between cellular energy status, cytosolic acidification and actin remodelling in pollen tubes. *New Phytol.* **236**: 1691-1707.
- Wang, L., Lin, Z., Triviño, M., Nowack, M.K., Franklin-Tong, V.E., and Bosch, M. (2018). Self-incompatibility in *Papaver* pollen: programmed cell death in an acidic environment. *J. Exp. Bot.* **70**: 2113-2123.
- Wang, X., Wang, K., Liu, X., Liu, M., Cao, N., Duan, Y., Yin, G., Gao, H., Wang, W., Ge, W., Wang, J., Li, R., and Guo, Y. (2017). Pollen-expressed leucin-rich-repeat extensins are essential for pollen germination and growth. *Plant Physiol.* **176**: 1993-2006.
- Wheeler, M.J., de Graaf, B.H.J., Hadjosif, N., Perry, R.M., Poulter, N.S., Osman, K., Vatovec, S., Harper, A., Franklin, F.C.H., and Franklin-tong, V.E. (2009). Identification of the pollen self-incompatibility determinant in *Papaver rhoeas*. *Nature* **459**: 992-995.
- Willats, W.G.T., Orfila, C., Limberg, G., Buchholt, H.C., van Alebeek, G.J., Voragen, A.G., Marcus, S.E., Christensen, T.M., Mikkelsen, J.D., Murray, B.S., Knox, J.P. (2001). Modulation of the degree and pattern of methyl-esterification of pectic homogalacturonan in plant cell Walls. *J. Biol. Chem.* **276**: 19404-19413.
- Willats, W.G.T., Marcus, S.E., and Knox, J.P. (1998). Generation of a monoclonal antibody specific to (1→5)- $\alpha$ -L-arabinan. *Carbohydr. Res.* **308**: 149-152.
- Xie, Q., Wang, P., Liu, X., Yuan, L., Wang, L., Zhang, C., Li, Y., Xing, H., Zhi, L., Yue, Z. Zhao, C., McClung C.R., and Xu, X. (2014). LNK1 and LNK2 are transcriptional coactivators in the *Arabidopsis* circadian oscillator. *Plant Cell* **26**: 2843-2857.
- Yang, Q., Meng, D., Gu, Z., Li, W., Chen, Q., Li, Y., Yuan, H., Yu, J., Liu, C., and Li, T. (2018).

---

Apple S-RNase interacts with an actin-binding protein, MdMVG, to reduce pollen tube growth by inhibiting its actin-severing activity at the early stage of self-pollination induction. *Plant J.* **95**: 41-56.

**Zhang, Z., Zhang, B., Chen, Z., Zhang, D., Zhang, H., Wang, H., Zhang, Y., Cai, D., Liu, J., Xiao, S., Huo, Y., Liu, J., Zhang, L., Wang, M., Liu, X., Xue, Y., Zhao, L., Zhou, Y., and Chen, H.** (2018). A *PECTIN METHYLESTERASE* gene at the maize *Ga1* locus confers male function in unilateral cross-incompatibility. *Nat. Commun.* **9**: 3678.

**Zhao, H., Song, Y., Li, J., Zhang, Y., Huang, H., Li, Q., Zhang, Y., and Xue, Y.** (2021a). Primary restriction of S-RNase cytotoxicity by a stepwise ubiquitination and degradation pathway in *Petunia hybrida*. *New Phytol.* **231**: 1249-1264.

**Zhao, H., Zhang, Y., Zhang, H., Song, Y., Zhao, F., Zhang, Y.e., Zhu, S., Zhang, H., Zhou, Z., Guo, H., et al.** (2021b). Origin, loss and regain of self-incompatibility in angiosperms. *Plant Cell.* **34**: 579-596.

**Zhou, H., Yin, H., Chen, J., Liu, X., Gao, Y., Wu, J., and Zhang, S.** (2016). Gene-expression profile of developing pollen tube of *Pyrus bretschneideri*. *Gene Expr. Patterns* **20**: 11-21.

**Zhou, X., Lu, J., Zhang, Y., Guo, J., Lin, W., Van Norman, J.M., Qin, Y., Zhu, X., and Yang, Z.** (2021). Membrane receptor-mediated mechano-transduction maintains cell integrity during pollen tube growth within the pistil. *Dev. Cell* **56**: 1030-1042. e6.

**Zhou, Z., Bi, G., and Zhou, J.** (2018). Luciferase complementation assay for protein-protein interactions in plants. *Curr. Protoc. Plant Biol.* **3**: 42-50.

**Zhu, Y., Zou, X., Dean, A.E., O'Brien, J., Gao, Y., Tran, E.L., Park, S.H., Liu, G., Kieffer, M.B., Jiang, H., Stauffer, M.E., Hart, R., Quan, S., Satchell, K.J.F., Horikoshi, N., Bonini, M., and Gius, D.** (2019). Lysine 68 acetylation directs MnSOD as a tetrameric detoxification complex versus a monomeric tumor promoter. *Nat. Commun.* **10**: 2399.

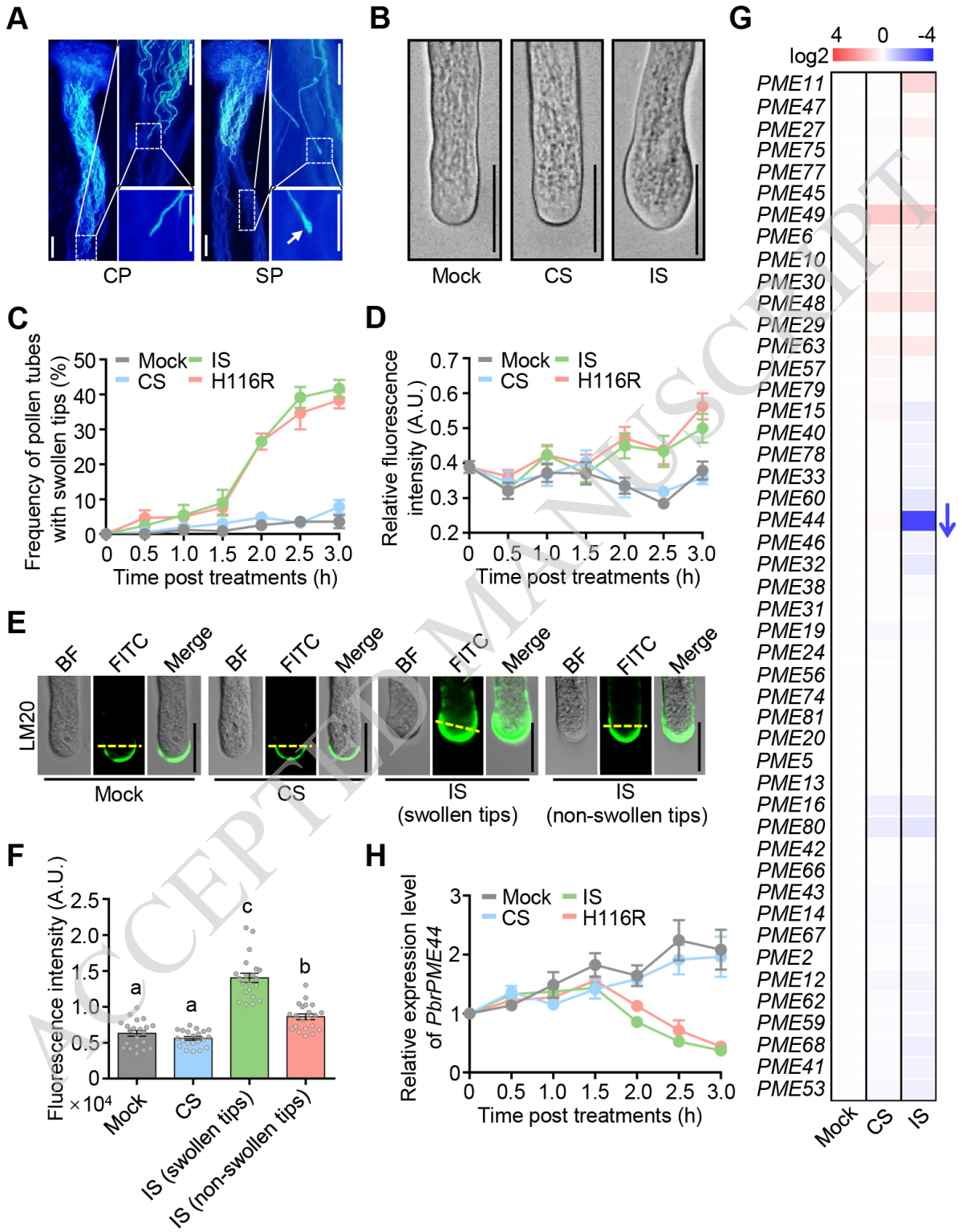


**Figure 1. PbrS-RNase induces swelling at the tips of pollen tubes and suppresses *PbrPME44* expression during the self-incompatibility response.**

**(A)** Aniline blue staining of *Pyrus bretschneideri* cv. Dangshansuli pistils 48 h after pollination with *P. bretschneideri* cv. Huanghua pollen (cross-pollination, CP; compatible) and Dangshansuli pollen (self-pollination, SP; incompatible). Insets showing high-magnification views of the boxed areas are shown on the right. The self-pollinated tubes in SP had swollen tips (white arrow). Scale bars, 100  $\mu$ m.

**(B)** His-tagged recombinant PbrS-RNases (rPbrS-RNases) induce the swelling of SI pollen tubes in vitro after a 2.5-h treatment. Mock, liquid germination medium; CS, compatible rPbrS-RNase; IS, incompatible rPbrS-RNase. Scale bars, 20  $\mu$ m.

**(C)** Time course analysis of the frequency of pollen tubes with swollen tips under mock, CS, IS, and H116R mutation treatments. H116R, incompatible rPbrS-RNases (rPbrS<sub>7</sub>-RNase<sup>H116R</sup> + rPbrS<sub>34</sub>-RNase<sup>H116R</sup>). Data are means  $\pm$  s.e.m.,  $n \geq 30$  pollen tubes.

**(D)** Quantitative analysis of the time course of fluorescence intensity of the LM20 antibody at the apical region (the area within 5  $\mu$ m from the tip to the shank) of pollen tubes under mock, CS, IS and H116R mutation treatments. Data are means  $\pm$  s.e.m.,  $n = 20$  pollen tubes.

**(E)** rPbrS-RNases induce an increase in the level of methyl esterified pectin in pollen tubes 2 h after mock, CS, and IS treatments regardless of whether the tips were swollen. Methyl esterified pectins in the pollen tube were immunolabeled with LM20. BF, brightfield image; FITC, Anti-rat IgG-FITC antibody. Scale bars, 20  $\mu$ m.

**(F)** Quantitative analysis of the fluorescence intensity of LM20 at the apical regions of pollen tubes 2.0 h after mock, CS, and IS treatments. Data are means  $\pm$  s.e.m.,  $n \geq 20$  pollen tubes.

**(G)** Relative expression levels of 47 pollen-expressed *PbrPME* genes (Supplemental Table S2) 2.5 h after mock, CS, and IS treatments using the in vitro pollen culture system. Relative expression levels were normalized to that under mock treatment. The blue arrow indicates the only gene that was downregulated more than two-fold. *PbrTUB-2* was used as the reference gene. Data are means  $\pm$  s.e.m.,  $n = 3$  biological replicates.

**(H)** Time course analysis of the expression levels of *PbrPME44* in pollen tubes under mock, CS, IS, and H116R mutation treatments in vitro. For these treatments, pollen tubes (Dangshansuli; S<sub>7</sub> or S<sub>34</sub>) were pre-cultured in liquid germination medium for 1.5 h. *PbrTUB-2* was used as the reference gene for normalization. Data are means  $\pm$  s.e.m.,  $n = 7$  biological replicates. Statistical analysis results for all figures and supplemental figures are presented in Supplemental Data Set S4.

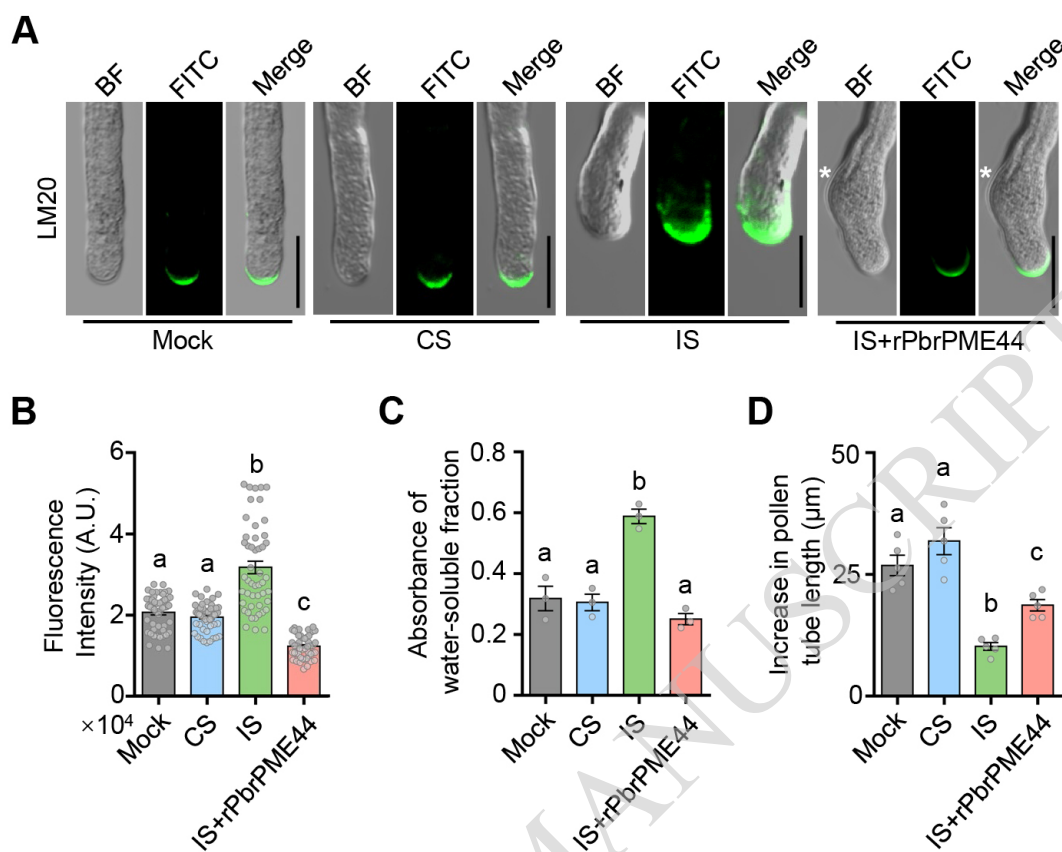


**Figure 2. PbrPME44 alleviates the PbrS-RNase-induced increase in methyl esterified pectin levels.**

(A) Methyl esterified pectins in the pollen tube were immunolabeled with the LM20 antibody 2 h after mock, CS, IS, and IS plus His-tagged recombinant PbrPME44 protein (rPbrPME44) treatments. For PME compensation experiments, pollen tubes were treated with rPbrS-RNases for 2 h, followed by the addition of rPbrPME44 and incubation for 1 h. The white asterisks indicate the positions of swelling. Mock, liquid germination medium; CS, compatible rPbrS-RNase; IS, incompatible rPbrS-RNase. BF, brightfield image; FITC, Anti-rat IgG-FITC antibody. Scale bars, 20 μm.

(B) Quantitative analysis of the fluorescence intensity of LM20 at the apical regions of the pollen tubes from (A). Different lowercase letters indicate significant differences, as determined by ANOVA followed by Tukey's multiple comparison test ( $P < 0.05$ ,  $n = 49$  pollen tubes). Data are means  $\pm$  s.e.m.

(C) Quantification of levels of methyl esterified pectins (using ELISA) in alcohol-insoluble residues extracted from pollen tubes under the treatments indicated in (A). Water was used as the elution buffer. The LM20 monoclonal antibody was used to detect methyl esterified pectins. Different lowercase letters indicate significant differences as determined by ANOVA followed by Tukey's multiple comparison test ( $P < 0.05$ ,  $n = 3$  biological replicates). Data are means  $\pm$  s.e.m.

(D) Quantitative analysis of the increase in pollen tube length under the indicated treatments in (A). Five biological replicates were performed, with each replicate containing at least 30 pollen tubes. Different lowercase letters indicate significant differences, as determined by ANOVA followed by Tukey's multiple comparison test ( $P < 0.05$ ). Data are means  $\pm$  s.e.m.

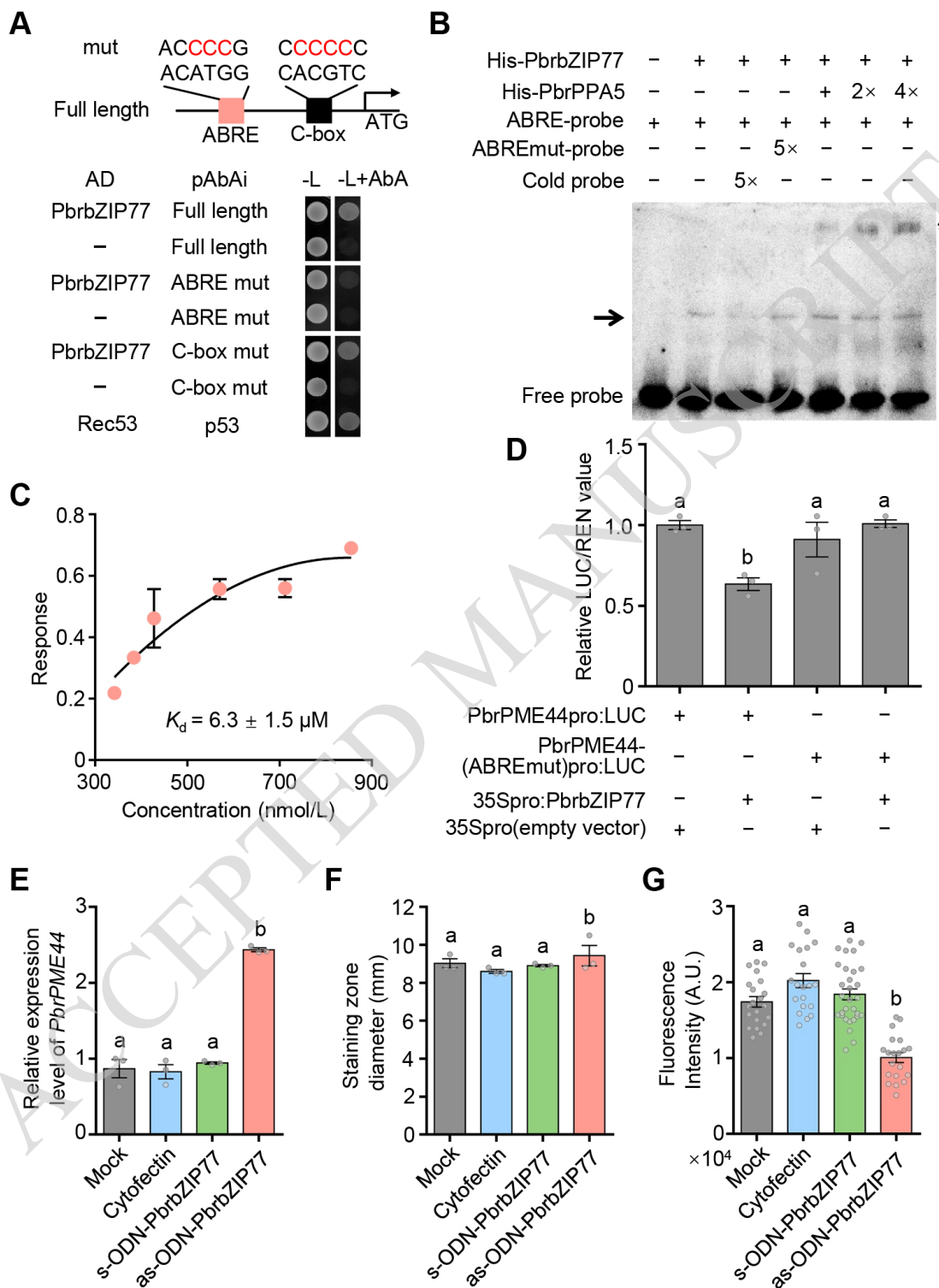


**Figure 3. PbrbZIP77 suppresses *PbrPME44* expression by binding to the ABRE in its promoter.**

**(A)** Yeast one-hybrid assays showing that the ABRE motif is essential for the binding of PbrbZIP77 to the *PbrPME44* promoter. The 1,300-bp sequence upstream of the start codon of *PbrPME44* was cloned into pAbAi as described in Materials and Methods. The pink box represents the ABA-responsive element (ACATGG) or its mutated form (ACCCCG). The black box represents the C-box element (CACGTC) or its mutated form (CCCCC).

**(B)** Binding of His-tagged recombinant PbrbZIP77 to the ABRE of the *PbrPME44* promoter region and a super-shift EMSA of the PbrPPA5–PbrbZIP77 complex. The 30-bp *PbrPME44* promoter fragment containing the ABRE was labeled with biotin and used as a probe. – represents absence; + represents presence; the black arrow indicates the shifted band; and the black asterisk indicates the super-shifted band.

**(C)** Quantification of the interaction between PbrbZIP77 and the 30-bp *PbrPME44* promoter fragment containing the ABRE using a biolayer interferometry (BLI) assay. Three technical replicates were performed.

**(D)** PbrbZIP77-repressed *PbrPME44* promoter activity depends on the ABRE in a dual-luciferase assay. The empty vector (35Spro) served as a negative control, and the LUC/REN ratio of 35Spro was set to 1. – represents absence and + represents presence. Different lowercase letters indicate significant differences, as determined by ANOVA followed by Tukey's multiple comparison test ( $P < 0.05$ ,  $n = 3$  biological replicates). Data represent the means  $\pm$  s.e.m.

**(E)** *PbrPME44* is upregulated in pollen tubes 2 h after treatment with antisense-oligodeoxynucleotide-PbrbZIP77 (as-ODN-PbrbZIP77). Cytofectin (Lipofectamine 2000) was used as the transfection reagent. The sense-oligodeoxynucleotide-PbrbZIP77 (s-ODN-PbrbZIP77) was used as the negative control. Mock, liquid germination medium. Different lowercase letters indicate significant differences, as determined by ANOVA followed by Tukey's multiple comparison test ( $P < 0.05$ ,  $n = 3$  biological replicates). Data are means  $\pm$  s.e.m.

**(F)** Analysis of total PME activity by ruthenium red staining under mock, cytofectin, s-ODN-PbrbZIP1, and as-ODN-PbrbZIP1 treatments. The diameters of the stained zones were measured with calipers. Different lowercase letters indicate significant differences, as determined by ANOVA followed by Tukey's multiple comparison test ( $P < 0.05$ ,  $n = 3$  biological replicates). Data are means  $\pm$  s.e.m.

**(G)** Quantitative analysis of the fluorescence intensity of LM20 at the apical regions of pollen tubes under mock, cytofectin, s-ODN-PbrbZIP1, and as-ODN-PbrbZIP1 treatments. Different lowercase letters indicate significant differences, as determined by ANOVA followed by Tukey's multiple comparison test ( $P < 0.05$ ,  $n \geq 20$  pollen tubes). Data are means  $\pm$  s.e.m.

ACCEPTED MANUSCRIPT

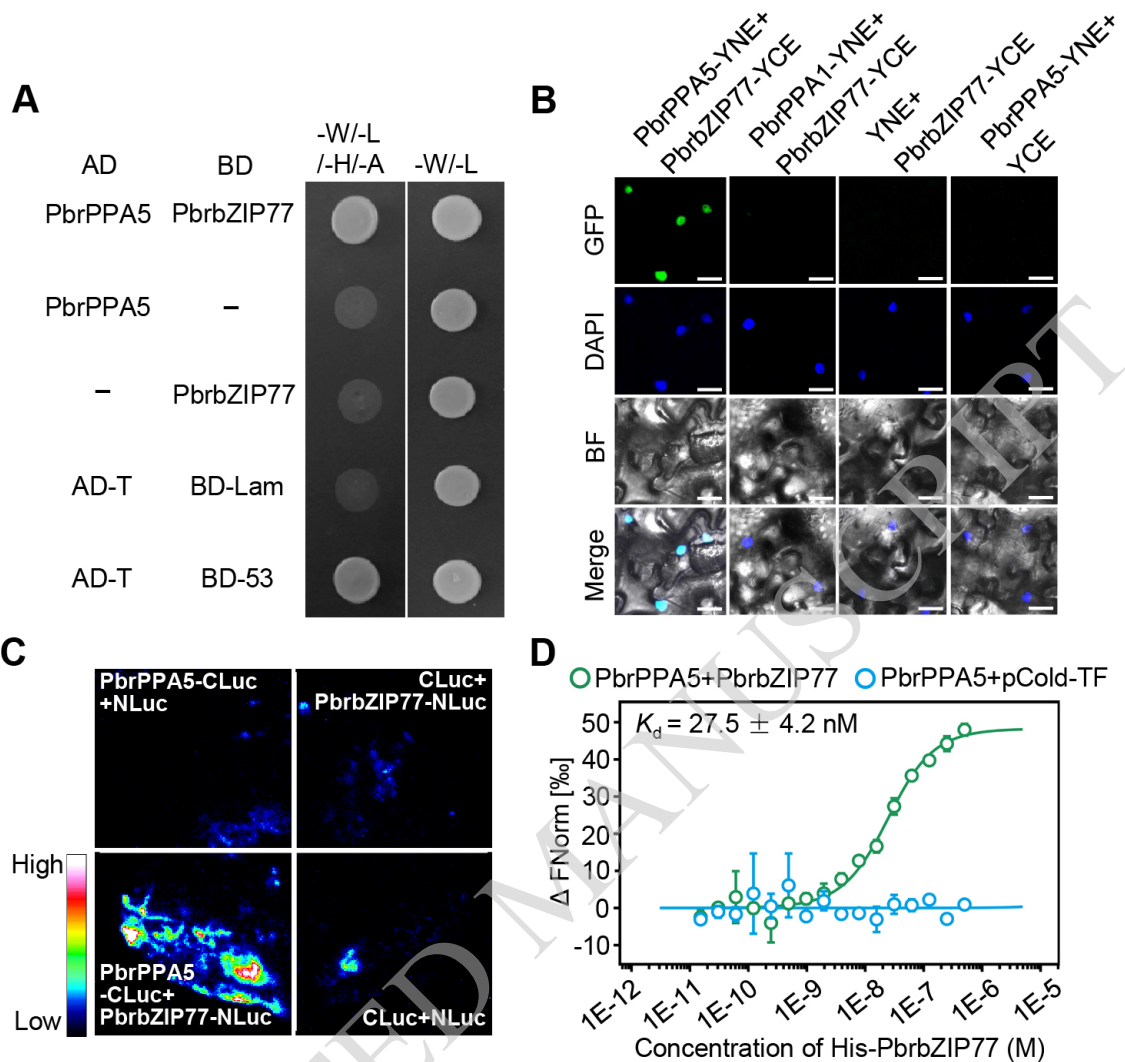


**Figure 4. PbrPPA5 interacts with PbrbZIP77 in vitro and in vivo.**

**(A)** Yeast two-hybrid assay of the interaction between PbrPPA5 (activation domain, AD) and PbrbZIP77 (binding domain, BD). Co-expression of pGBKT7-P53 and pGADT7-T was used as a positive control and that of pGBKT7-Lam and pGADT7-T as a negative control. Interactions were determined based on growth on synthetic defined (SD)-W-L-H-A (-Ade-Leu-Trp-His) medium.

**(B)** Bimolecular fluorescence complementation (BiFC) assays of the interaction between PbrbZIP77 and PbrPPA5 constructs in *N. benthamiana* leaves. Vectors YNE and YCE contain the N-terminal and C-terminal fragments of YFP, respectively. Scale bars, 20  $\mu\text{m}$ .

**(C)** Luciferase complementation imaging (LCI) assay of the interaction between PbrbZIP77 and PbrPPA5 in *N. benthamiana* leaves. NLuc, CLuc, vectors containing the N-terminal and C-terminal fragments of firefly luciferase, respectively. Co-infiltration of *35Spro:NLuc* and *35Spro:Cluc* was used as a negative control.

**(D)** Binding affinity assay showing the interaction kinetics (as indicated by  $K_d$  values) between His-tagged recombinant PbrPPA5 and His-PbrbZIP77, as measured by microscale thermophoresis (MST) analysis.

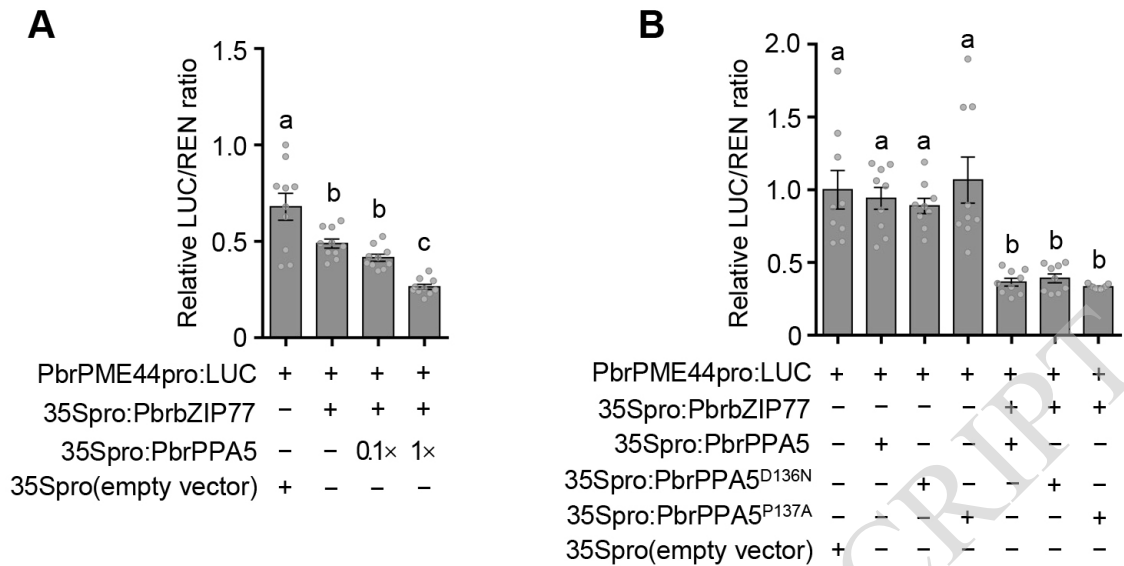


**Figure 5. PbrPPA5 enhances PbrbZIP77-mediated suppression of PbrPME44 expression.**

**(A)** PbrPPA5 promotes the PbrbZIP77-mediated suppression of *PbrPME44* expression in a concentration-dependent manner, as measured in a dual-luciferase assay. The empty vector (35Spro) served as a negative control, and the LUC/REN ratio of 35Spro was set to 1. The effector constructs consisted of the *PbrbZIP77* or *PbrPPA5* coding sequences driven by the 35S promoter; *PbrPME44pro:LUC* was used as the reporter construct. – represents absence, and + represents presence. Different lowercase letters indicate significant differences, as determined by ANOVA followed by Tukey's multiple comparison test ( $P < 0.05$ ,  $n = 10$  biological replicates). Data are means  $\pm$  s.e.m.

**(B)** The co-suppressor activity of PbrPPA5 for *PbrPME44* expression is independent of its sPPase activity. Dual-luciferase assays were performed using *N. benthamiana* leaves co-infiltrated with the reporter construct *PbrPME44pro:LUC* and the effector constructs 35Spro:*PbrbZIP77*, 35Spro:*PbrPPA5*, 35Spro:*PbrPPA5*<sup>D136N</sup>, 35Spro:*PbrPPA5*<sup>P137A</sup> and 35Spro (empty vector), as indicated. – represents absence and + represents presence. Different lowercase letters indicate significant differences, as determined by ANOVA followed by Tukey's multiple comparison test ( $P < 0.05$ ,  $n = 9$  biological replicates). Data are means  $\pm$  s.e.m.

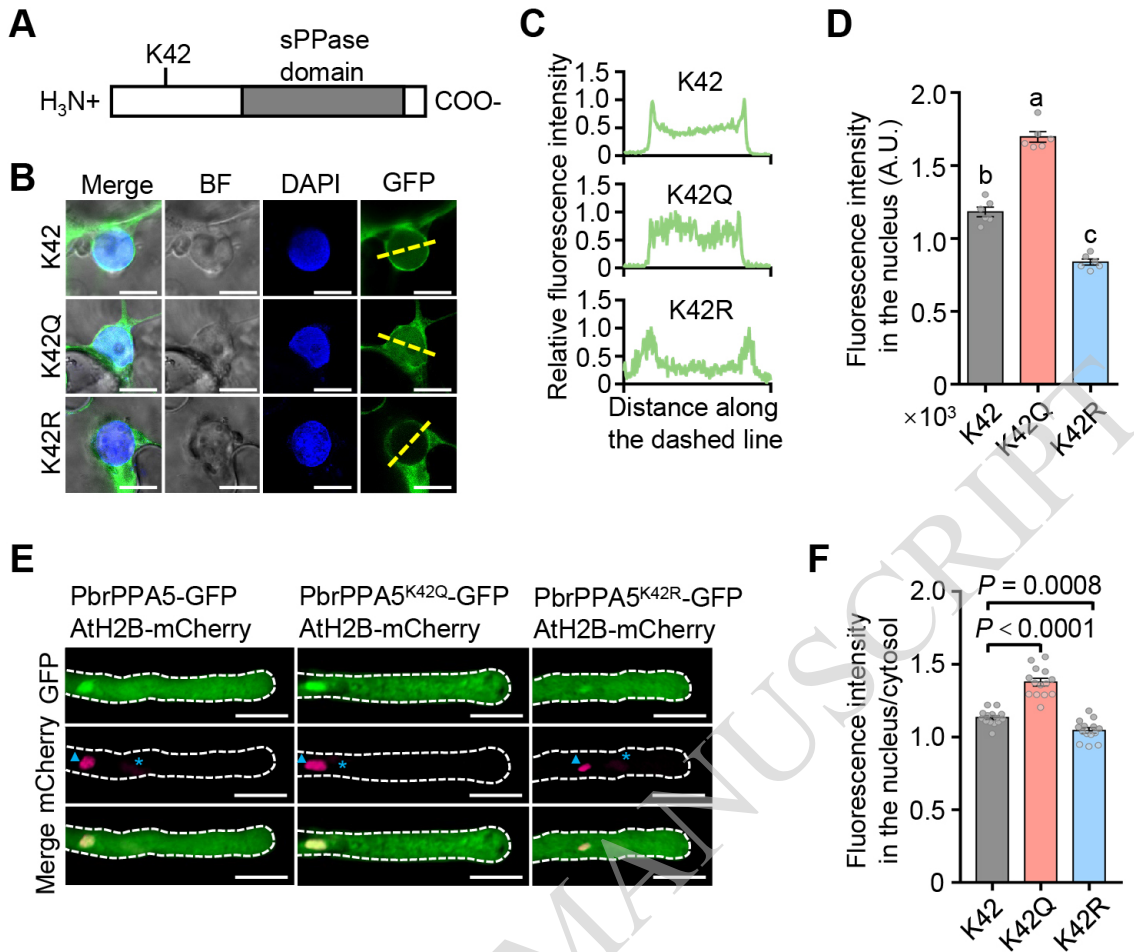


**Figure 6. Acetylation of the K42 residue in PbrPPA5 promotes accumulation of PbrPPA5 in the nucleus.**

**(A)** Structure of PbrPPA5 with the sPPase domain indicated. K42, the Lys residue at position 42 in the N-terminal region of PbrPPA5.

**(B)** Acetylation of the K42 residue in PbrPPA5 promotes its accumulation in the nucleus. Substitution of the K42 residue with a charge-conservative (positively charged) Arg residue (R) or an uncharged Glu residue (Q) mimics a nonacetylated or constitutively acetylated state, respectively. *PbrPPA5-GFP* (K42), *PbrPPA5<sup>K42Q</sup>-GFP* (K42Q), and *PbrPPA5<sup>K42R</sup>-GFP* (K42R) were transiently expressed in *N. benthamiana* leaves and observed under a confocal microscope. Green represents the fluorescence intensity of GFP; blue represents the fluorescence intensity of the nucleus marker 4',6-diamidino-2-phenylindole (DAPI). The yellow dashed lines represent the positions used to measure fluorescence intensity. Scale bars, 10  $\mu$ m.

**(C)** Quantitative analysis of the relative fluorescence intensity of GFP in the last column in (B). Fluorescence intensity of PbrPPA5-GFP was measured using ZEN software in the area across the yellow dashed line crossing the nucleus. The values on the x-axis represent the distance along the yellow dashed lines. The values on the y-axis represent the fluorescence intensity of PbrPPA5-GFP.

**(D)** Quantitative analysis of the fluorescence intensity of PbrPPA5-GFP in the nucleus. Different lowercase letters indicate significant differences, as determined by ANOVA followed by Tukey's multiple comparison test ( $P < 0.05$ ,  $n = 6$  leaf cells). Data are means  $\pm$  s.e.m.

**(E)** Images of the subcellular localization of PbrPPA5 and its mutant forms in pear pollen tubes. The expression of *PbrPPA5-GFP*, *PbrPPA5<sup>K42Q</sup>-GFP*, *PbrPPA5<sup>K42R</sup>-GFP* and *Ath2B-mCherry* was driven by the *NTP303* promoter. *PbrPPA5-GFP*, *PbrPPA5<sup>K42Q</sup>-GFP* and *PbrPPA5<sup>K42R</sup>-GFP* were transiently co-expressed with *Ath2B-mCherry* in pear pollen tubes by particle bombardment. The pollen was cultured for 4 h after transformation. The blue asterisk represents the vegetative nucleus and the blue triangle represents the generative nucleus. Scale bars, 20  $\mu$ m.

**(F)** Quantitative analysis of the ratio of fluorescence intensity in the nucleus/cytosol for PbrPPA5-GFP, PbrPPA5<sup>K42Q</sup>-GFP and PbrPPA5<sup>K42R</sup>-GFP in the nuclei of pollen tubes from (E).  $P$ -values were obtained by Student's  $t$ -test. Data are means  $\pm$  s.e.m.,  $n = 10$  pollen tubes.

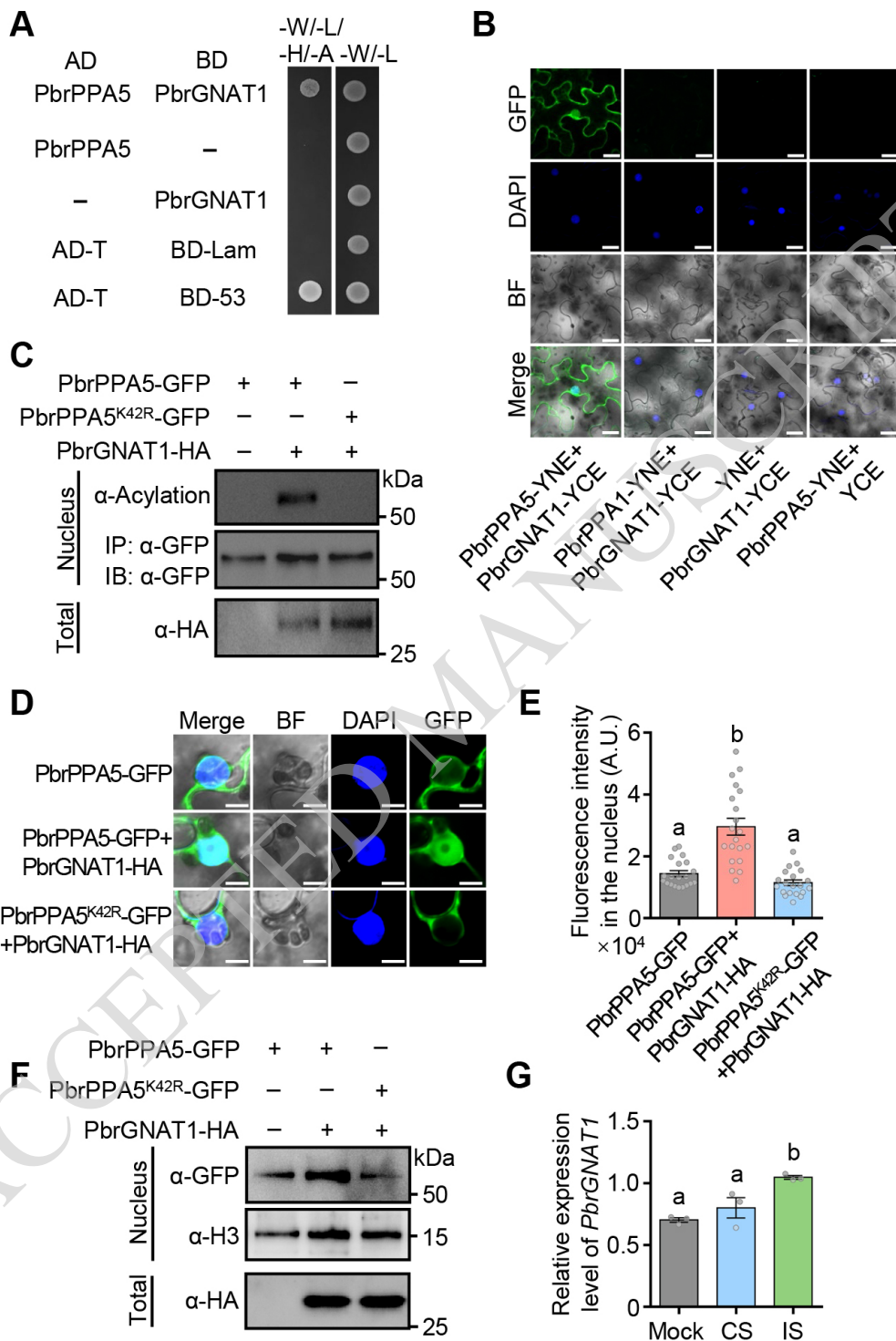


**Figure 7. PbrGNAT1 acetylates PbrPPA5 and promotes its nuclear accumulation.**

**(A)** Yeast two-hybrid assay of the interactions between PbrPPA5 (activation domain, AD) and PbrGNAT1 (binding domain, BD). Co-expression of pGBKT7-P53 and pGADT7-T was used as a positive control and that of pGBKT7-Lam and pGADT7-T as a negative control. Interactions were determined based on growth on SD/-W-L-H-A (-Ade-Leu-Trp-His) medium.

**(B)** BiFC assays of the interaction between PbrPPA5 and PbrGNAT1 in *N. benthamiana* leaves. Vectors YNE and YCE contain the N-terminal and C-terminal fragments of YFP, respectively. Scale bars, 20  $\mu$ m.

**(C)** PbrGNAT1 acetylates the K42 residue of PbrPPA5 in vivo. Substitution of K42 with a charge-conservative Arg residue (R) mimics a nonacetylated state. *PbrGNAT1-HA* with *PbrPPA5-GFP* or *PbrPPA5<sup>K42R</sup>-GFP* were transiently co-expressed in *N. benthamiana* leaves. Nuclear proteins were extracted and immunoprecipitated with magnetic beads containing  $\alpha$ -GFP antibody. The protein extracts were immunoblotted with an  $\alpha$ -acetylation antibody. The abundance of PbrGNAT1-HA, PbrPPA5-GFP and PbrPPA5<sup>K42R</sup>-GFP was verified using an  $\alpha$ -HA antibody and an  $\alpha$ -GFP antibody, respectively.  $\alpha$ -GFP was used as the loading control for nuclear proteins.

**(D)** Co-expression of *PbrGNAT1* and *PbrPPA5* promotes the accumulation of PbrPPA5 in the nucleus. *PbrGNAT1-HA* with *PbrPPA5-GFP* or *PbrPPA5<sup>K42R</sup>-GFP* were transiently expressed in *N. benthamiana* leaves. The fluorescence of their encoded proteins was observed under a confocal microscope. Green represents the fluorescence intensity of GFP; blue represents the fluorescence intensity of the nuclear marker 4',6-diamidino-2-phenylindole (DAPI). Scale bars, 10  $\mu$ m.

**(E)** Quantitative analysis of the fluorescence intensity in the nucleus of PbrPPA5-GFP from (D). Different lowercase letters indicate significant differences, as determined by ANOVA followed by Tukey's multiple comparison test ( $P < 0.05$ ,  $n = 20$  leaf cells). Data represent means  $\pm$  s.e.m.

**(F)** Immunoblot analysis of PbrPPA5 in the nucleus from transiently infiltrated *N. benthamiana* leaves with or without co-expression of PbrGNAT1-HA. PbrPPA5-GFP and PbrPPA5<sup>K42R</sup>-GFP were detected using an  $\alpha$ -GFP antibody, and an  $\alpha$ -H3 antibody was used as the loading control for nuclear proteins. The expression of PbrGNAT1-HA in total leaf protein was detected using an  $\alpha$ -HA antibody.

**(G)** The expression levels of *PbrGNAT1* in pollen tubes under 1 h mock, CS and IS treatments in vitro. Mock, liquid germination medium; CS, compatible rPbrS-RNase; IS, incompatible rPbrS-RNase. *PbrTUB-2* was used as the reference gene for normalization. Different lowercase letters indicate significant differences, as determined by ANOVA followed by Tukey's multiple comparison test ( $P < 0.05$ ,  $n = 3$  biological replicates). Data are means  $\pm$  s.e.m.

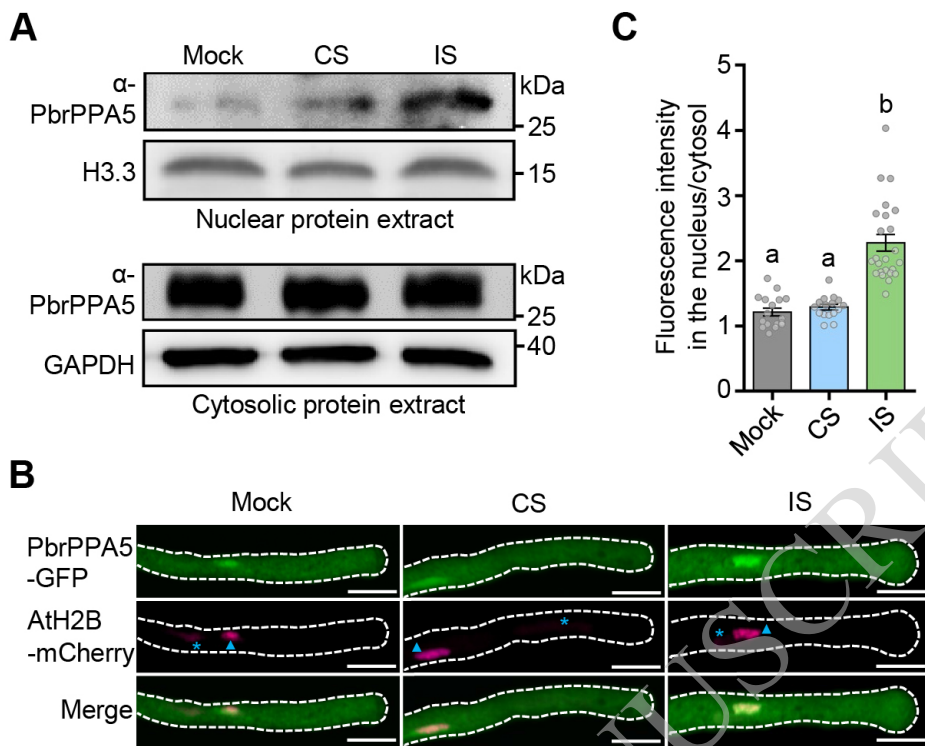


**Figure 8. SI induces PbrPPA5 accumulation in the nucleus.**

**(A)** immunoblot analysis showing that 1.5 h of IS treatment induces PbrPPA5 accumulation in the nucleus. Nucleus/cytosolic soluble fractions were isolated from pear pollen.  $\alpha$ -H3.3 and  $\alpha$ -GAPDH antibodies were used as the loading controls for nuclear and cytoplasmic proteins, respectively. Mock, liquid germination medium; CS, compatible rPbrS-RNase; IS, incompatible rPbrS-RNase.

**(B)** Images of the SI-induced PbrPPA5 accumulation in the nuclei of pollen tubes 1.5 h after IS treatment. The expression of *PbrPPA5-GFP* and *AtH2B-mCherry* was driven by the *NTP303* promoter, and *PbrPPA5-GFP* and *AtH2B-mCherry* was transiently co-expressed in pear pollen tubes by particle bombardment. The transformed pear pollen was cultured for 3 h and then treated for 1.5 h with mock, CS, and IS treatments. The blue asterisks represent the vegetative nuclei and the blue triangles represent the generative nuclei. Scale bars, 20  $\mu$ m.

**(C)** Quantitative analysis of the ratio of fluorescence intensity of PbrPPA5-GFP in the nucleus/cytoplasm in the nuclei of pollen tubes from (B). Different lowercase letters indicate significant differences, as determined by ANOVA followed by Tukey's multiple comparison test ( $P < 0.05$ ,  $n \geq 12$  pollen tubes). Data are means  $\pm$  s.e.m.

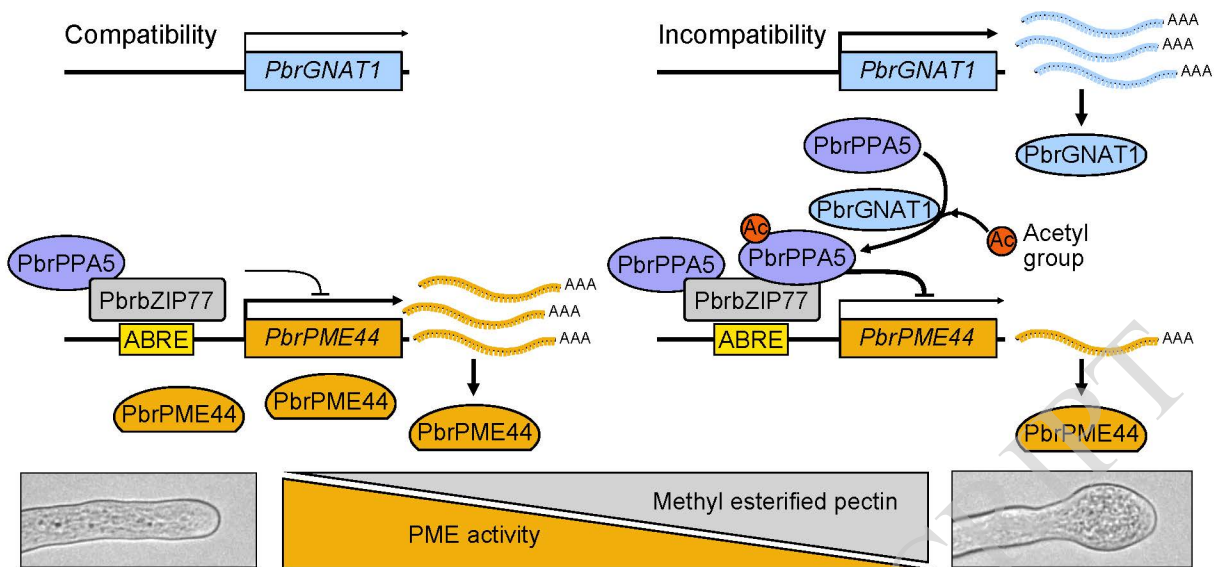


**Figure 9 A working model for the role of PbrPPA5 in tip swelling of pear pollen tubes under SI challenge.** In growing pollen tubes, PbrPPA5 interacts with PbrbZIP77, and the PbrPPA5-PbrbZIP77 complex suppresses the expression of *PbrPME44* by binding to the ABRE in its promoter to maintain the balance between methyl esterified and de-esterified pectin levels in pollen tubes. During the SI response, the expression level of *PbrGNAT1* increases, and PbrGNAT1 acetylates PbrPPA5, inducing the accumulation of PbrPPA5 in the nucleus. PbrPPA5 in the nucleus binds to PbrbZIP77 to enhance the repression of *PbrPME44*. The downregulation of *PbrPME44* leads to an increase in methyl esterified pectin levels in the pollen tube cell wall, resulting in swelling at the tips of pollen tubes.